



**Analysis of multielectron, multistep homogeneous catalysis  
by rotating disc electrode voltammetry: Theory, application,  
and obstacles**

Journal:	<i>Analyst</i>
Manuscript ID	AN-ART-10-2019-002192.R1
Article Type:	Paper
Date Submitted by the Author:	20-Dec-2019
Complete List of Authors:	Lee, Katherine; University of North Carolina, Chemistry Gruninger, Cole; University of North Carolina, Chemistry Lodaya, Kunal; University of North Carolina, Chemistry Qadeer, Saad; University of North Carolina, Chemistry Griffith, Boyce; University of North Carolina, Chemistry Dempsey, Jillian; University of North Carolina, Chemistry

# Analysis of multielectron, multistep homogeneous catalysis by rotating disc electrode voltammetry: Theory, application, and obstacles

Katherine J. Lee,<sup>†</sup> Cole T. Gruninger,<sup>†</sup> Kunal M. Lodaya,<sup>†</sup> Saad Qadeer,<sup>‡</sup> Boyce E. Griffith,<sup>‡</sup>  
and Jillian L. Dempsey<sup>†</sup>

<sup>†</sup>Department of Chemistry, University of North Carolina at Chapel Hill, Chapel Hill, North  
Carolina, USA 27599

<sup>‡</sup>Department of Mathematics, University of North Carolina at Chapel Hill, Chapel Hill, North  
Carolina, USA 27599

## ABSTRACT

Rotating disc electrode (RDE) voltammetry has been widely adopted for the study of heterogenized molecular electrocatalysts for multi-step fuel-forming reactions but this tool has never been comprehensively applied to their homogeneous analogues. Here, the utility and limitations of RDE techniques for mechanistic and kinetic analysis of homogeneous molecular catalysts that mediate multi-electron, multi-substrate redox transformations are explored. Using the ECEC' reaction mechanism as a case study, two theoretical models are derived based on the Nernst diffusion layer model and the Hale transformation. Current-potential curves generated by these computational strategies are compared under a variety of limiting conditions to identify conditions under which the more minimalist Nernst Diffusion Layer approach can be applied. Based on this theoretical treatment, strategies for extracting kinetic information from the plateau current and the foot of the catalytic wave are derived. RDEV is applied to a cobaloxime hydrogen evolution reaction (HER) catalyst under non-aqueous conditions in order to experimentally validate this theoretical framework and explore the feasibility of RDE as a tool for studying homogeneous catalysts. Crucially, analysis of the foot-of-the-wave via this theoretical framework provides rate constants for elementary reaction steps that agree with those extracted from stationary voltammetric methods, supporting the application of RDE to study homogeneous fuel-forming catalysts. Finally, obstacles encountered during the kinetic analysis of cobaloxime, along with the voltammetric signatures that used to diagnose this reactivity, are discussed with the goal of guiding groups working to improve RDE set-ups and help researchers avoid misinterpretation of RDE data.

## INTRODUCTION

The increasingly dire outlook for communities and economies across the planet as global temperatures continue to rise has crystallized the need for the scientific community to develop renewable-energy based alternatives to fossil fuels.<sup>1-3</sup> Towards this goal, significant research has focused on improving methods for capturing energy from renewable sources and converting this energy into a storable and transportable form.<sup>4,5</sup> While energy harvesting technology is approaching broad-scale feasibility, energy storage remains a significant bottleneck.<sup>6</sup> A promising storage strategy uses renewable energy to power electrocatalytic reactions which generate energy-rich fuels (e.g. H<sub>2</sub>, CH<sub>3</sub>OH) from energy-poor precursors (e.g. H<sub>2</sub>O, CO<sub>2</sub>). However, improved electrocatalytic systems are necessary for renewable energy-derived fuels to become economically competitive.<sup>7,8</sup>

Molecular transition metal-based electrocatalysts – which can be freely diffusing in solution or tethered to an electrode surface – have garnered considerable attention as their versatile molecular properties allow catalytic properties to be fine-tuned.<sup>9</sup> Intelligently improving these systems requires a deep understanding of the factors that dictate activity, selectivity, and stability, information which can be derived from experimental and computational analysis of reaction mechanisms.<sup>10,11</sup> Critical to this understanding is the ability to study the catalyst under operating conditions. This can be accomplished using a myriad of electrochemical characterization techniques, one of the most ubiquitous of which is cyclic voltammetry (CV).<sup>12,13</sup> The popularity of CV stems from the large time window in which accurate data can be extracted which facilitates kinetic characterization of fast processes, the relative affordability of the necessary equipment, and the availability of increasingly sophisticated models for the quantitative interpretation of voltammograms which can account for and provide insight into a growing number of kinetic, thermodynamic, and mechanistic factors.<sup>12,14-20</sup> However, there remains a need for advanced characterization techniques which can be coupled with real-time detection of products or reactive intermediates.<sup>8</sup>

In this respect, hydrodynamic electrochemical set-ups have extraordinary potential as many of these configurations are easily modified to generate dual electrode set-ups that allow continuous monitoring of the flowing solution.<sup>21</sup> While a diverse configuration of electrode set-ups and flow

1 patterns can be envisioned, these constructions are realistically limited by the need for reproducible  
2 mass-transfer conditions if rigorous theoretical treatment of these systems is to be accomplished.<sup>22</sup>  
3  
4 Of these convective electrode systems, the rotating disc electrode (RDE) is one of the few for which  
5  
6 rigorous mathematical models have been derived.<sup>12,23</sup> As the name suggests, the RDE is rotated at  
7  
8 a set frequency resulting in a steady flow of solution normal to the electrode. Upon reaching the  
9  
10 surface, the centrifugal force induced by the rotating electrode propels the solution outward in a radial  
11  
12 direction. The rotation speed of the RDE – which dictates the rate of mass transfer – provides a  
13  
14 parameter via which the kinetics and mechanism of homogeneous chemical processes can be  
15  
16 probed. It should be noted that the range of available rotational speed is typically limited from ca. 10  
17  
18 – 1000 rad sec<sup>-1</sup>, with the lower limit dictated by the need to achieve steady-state conditions and the  
19  
20 upper limit governed by the onset of turbulent flow.<sup>24,25</sup> This upper limit stymies kinetic  
21  
22 characterization of fast chemical processes and allows access to a smaller range of rate constants  
23  
24 relative to stationary CV, which relies on scan rate – a parameter which can be varied over a far larger  
25  
26 range – as a kinetic probe.<sup>14</sup> However, the steady-state conditions achieved during RDE  
27  
28 measurements can amplify the observed current densities relative to stationary set-ups while also  
29  
30 eliminating the capacitive currents which can greatly distort CV measurements at high scan rate,  
31  
32 especially when employing low concentrations of substrate. Importantly, addition of an independent  
33  
34 ring electrode surrounding the central disc, a set-up known as a rotating ring-disc electrode (RRDE),  
35  
36 allows the analytes in the liquid flowing outward from the disc to be electrochemically monitored.<sup>21,26</sup>  
37  
38  
39  
40

41 Techniques based on RDE and RRDE electrochemistry have already found extensive  
42  
43 application in the evaluation of surface-adsorbed catalysts and heterogeneous electrocatalytic  
44  
45 materials.<sup>14,27,28</sup> In contrast, these tools have found a far cooler reception in the homogeneous  
46  
47 electrocatalytic community, though occasional reports using RDE or RRDE have trickled through.<sup>29–</sup>  
48  
49

50 <sup>34</sup> This is surprising considering the flurry of activity surrounding RDE voltammetry (RDEV) witnessed  
51  
52 in the 1980s and 90s which resulted in a large body of work describing the theoretical treatment of  
53  
54 RDE voltammograms for an array of homogeneous processes with coupled chemical steps,<sup>24,35,36</sup>  
55  
56  
57  
58  
59  
60

1 including a number of reports on one-electron, one-substrate EC' catalytic reactions.<sup>37–39</sup> However,  
2 this work was never extended to the multi-substrate, multi-electron reactions pertinent to fuel-forming  
3 processes.  
4  
5  
6  
7

8 Intrigued by this body of literature and motivated by the desire to assess the efficacy of this  
9 tool as a means of studying homogeneous electrocatalysis, we have critically evaluated the utility of  
10 RDEV for evaluating multi-step catalytic reactions. This report is divided into three parts. Part 1  
11 describes our theoretical treatment of this topic and includes a general overview of seminal work on  
12 the EC' mechanism, derives theoretical models for analyzing and digitally simulating RDE  
13 voltammograms of homogeneous multi-step catalysis, and discusses the parameters governing these  
14 catalytic responses. Parts 2 and 3 showcase our attempt to apply this tool in a real-world setting using  
15 a well-studied cobaloxime hydrogen evolution reaction (HER) electrocatalyst, with Part 2 discussing  
16 the theory and application of various analytical strategies and Part 3 focusing on the obstacles  
17 encountered during our adventure in the world of RDE. It should be noted that the theoretical  
18 framework derived in Part 1 focuses on the reported ECEC' mechanism of this model system;  
19 however, we hope our detailed discussion of the modeling process will allow readers to extend these  
20 derivations to other reaction schemes relevant to their own research. We also hope our holistic  
21 approach that identifies both the obstacles and opportunities presented by RDEV will inform next  
22 generation technology and ensure appropriate application of these cutting-edge strategies.  
23  
24  
25  
26  
27  
28  
29  
30  
31  
32  
33  
34  
35  
36  
37  
38

## 39 **EXPERIMENTAL**

40 **General Considerations.** All chemical syntheses were performed using either a nitrogen-filled  
41 glovebox or a high-vacuum manifold with standard Schlenk techniques. Solvents were degassed with  
42 argon and dried using a solvent system (Pure Process Technology). Water for polishing was obtained  
43 from a Milli-Q system. Tetrabutylammonium hexafluorophosphate (TCl, > 98%) was recrystallized  
44 from hot ethanol, washed with cold ethanol, and dried under vacuum for 8 hours at 80°C.  
45  
46  
47  
48  
49

50  $\text{Co}(\text{dmgBF}_2)_2(\text{H}_2\text{O})_2$  was synthesized and recrystallized according to literature methods and  
51 characterized via UV-vis absorbance spectroscopy.<sup>40</sup> Absorbance measurements were taken using  
52 an Agilent Cary 60 UV-vis spectrometer. Anilinium tetrafluoroborate,<sup>41</sup> 4-methoxyanilinium  
53  
54  
55  
56  
57  
58  
59  
60

1 tetrafluoroborate,<sup>41</sup> and 4-trifluoromethoxyanilinium tetrafluoroborate<sup>42</sup> were prepared according to  
2 literature methods.  
3  
4

5 **Electrochemical Methods.** All electrochemical measurements were performed in a nitrogen-filled  
6 glovebox using electrode leads that were fed through a custom port and connected to a WaveDriver  
7 potentiostat (Pine Research Instrumentation). Experiments were conducted in a 150 mL glass cell  
8 (Pine Research Instrumentation, model: RRP310) with a WaveVortex 10 electrode rotator (Pine  
9 Research Instrumentation, model: AF01WV10). Measurements were performed using a standard  
10 three-electrode configuration with the platinum wire counter electrode and silver wire  
11 pseudoreference electrode immersed in glass tubes filled with 0.25 M [NBu<sub>4</sub>][PF<sub>6</sub>] acetonitrile and  
12 isolated from the main cell compartment via a porous glass frit. Glassy carbon working electrodes  
13 (Pine Research Instrumentation, 5 mm OD, model: AFE5T050GCPK) were polished using a Milli-Q  
14 water slurry of 0.05 μm polishing powder (CH Instruments, no agglomerating agents), rinsed and  
15 sonicated in Milli-Q water, and rinsed with acetone. Working electrodes were electrochemically  
16 pretreated with three cyclic scans between 0.7 V to -2.8 V vs Fc<sup>+0</sup> couple (approximately) at 0.1 V  
17 s<sup>-1</sup> in 0.25 M [NBu<sub>4</sub>][PF<sub>6</sub>] acetonitrile solution. All RDE voltammograms used for quantitative  
18 measurements were collected with a newly cleaned and pretreated working electrode in a fresh  
19 solution unless otherwise noted. All voltammograms were recorded in 0.25 M [Bu<sub>4</sub>][PF<sub>6</sub>] acetonitrile  
20 solution and internally referenced to ferrocene.  
21  
22

23 Electrochemical simulations were performed using DigiElch Version 8.FD (Gamry) and MATLAB (The  
24 Mathworks). MATLAB simulations were carried out using custom prepared scripts utilizing a fully  
25 implicit finite difference formula paired with standard Newton-Raphson method to solve the resulting  
26 nonlinear reaction-convection-diffusion equations. See Supporting Information I.  
27  
28

## 29 RESULTS AND DISCUSSION

### 30 Glossary of Symbols

---

31 *A*: geometric electrode surface area (cm<sup>2</sup>)

32 *C*<sub>A</sub><sup>0</sup>: bulk concentration of acid

33 *C*<sub>P</sub><sup>0</sup>: bulk concentration of catalyst

1  $c_j$ : concentration  
 2  
 3  $D_{species}$ : diffusion coefficient of the subscript species ( $\text{cm}^2 \text{s}^{-1}$ )  
 4  
 5  $E$ : potential (V)  
 6  
 7  $E_{1/2}$ : half-wave potential (V)  
 8  
 9  $E_{couple}^0$ : standard potential of the couple denoted in the subscript (V)  
 10  
 11  $E_n$ : formal potential for the nth electron transfer in a catalytic cycle (V)  
 12  
 13  $\Delta E$ : potential difference between  $E_2$  and  $E_1$  (V), e.g.,  $\Delta E = E_2 - E_1$   
 14  
 15  $F$ : Faraday's constant  
 16  
 17 Fc: Ferrocene  
 18  
 19 Fc\*: Decamethylferrocene  
 20  
 21  $f$ :  $F/RT$  ( $\text{V}^{-1}$ )  
 22  
 23  $J_j(x)$ : mass transfer flux  
 24  
 25  $k$ : rate constant for a chemical step  
 26  
 27  $k_e$ : homogeneous electron transfer rate constant  
 28  
 29  $k_{FOWA}$ : observed rate constant extracted using FOWA  
 30  
 31  $k_{obs}$ : observed rate constant  
 32  
 33  $k_s$ : standard heterogeneous electrochemical rate constant ( $\text{cm s}^{-1}$ )  
 34  
 35  $i_c$ : observed catalytic current (A)  
 36  
 37  $i_p$ : diffusion-controlled plateau current of catalyst (A)  
 38  
 39  $i_{peak}$ : diffusion-controlled peak current of catalyst (A)  
 40  
 41  $i_{pl}$ : plateau current (A)  
 42  
 43  $n$ : number of electrons transferred at the electrode in the redox event  
 44  
 45  $R$ : gas constant  
 46  
 47  $T$ : Temperature (K)  
 48  
 49  $x$ : distance from the electrode surface  
 50  
 51  $v$ : solution velocity  
 52  
 53  $z_j$ : charge of species j  
 54  
 55  $\alpha$ : transfer coefficient  
 56  
 57  $\gamma$ : excess factor,  $\gamma = C_A^0/C_P^0$   
 58  
 59  $\delta$ : thickness of diffusion layer, for RDEV  $\delta = 1.61D^{1/3}v^{1/6}\omega^{-1/2}$  (cm)  
 60  
 in stationary CV  $\delta = (DRT/Fv)^{1/2}$  (cm)  
 61  
 62  $\theta$ : dimensionless potential scale,  $\theta = - (f)(E - E_{couple}^0)$   
 63  
 64  $\theta_{1/2}$ : dimensionless half-wave potential,  $\theta = - (f)(E_{1/2} - E_{couple}^0)$

- 1  $\lambda$ : dimensionless kinetic parameter,  $\lambda = (\delta/\mu)^2$   
 2  
 3  $\mu$ : thickness of reaction-diffusion layer,  $\mu = (D_{cat}/k)^{1/2}$  (cm)  
 4  
 5  $\nu$ : kinematic viscosity (cm s<sup>-1</sup>)  
 6  
 7  $v$ : scan rate (V s<sup>-1</sup>)  
 8  
 9  $\phi$ : electrical potential  
 10  
 11  $\Psi$ : dimensionless current,  $\Psi = i/i_p$   
 12  
 13  $\Psi^\infty$ : dimensionless plateau current,  $\Psi^\infty = i_c/i_p$   
 14  
 15  $\omega$ : rotation rate (rad s<sup>-1</sup>)  
 16

## 1. Waveshape analysis and mathematical modelling for homogeneous catalysis

---

### 1.1 Theoretical approaches for modeling electrochemical processes at the RDE

Theoretical treatment of any convective system requires solutions for a series of relevant mass-transport equations.<sup>12</sup> Mass transfer of a species to an electrode is governed by the Nernst-Planck equation which can be written for one-dimensional mass transfer as:

$$J_j(x) = -D_j \frac{dc_j}{dx} - z_j f D_j c_j \frac{d\phi(x)}{dx} + c_j v(x) \quad (1)$$

The three terms on the right-hand side of equation 1 represent the contributions to the mass transfer flux  $J_j(x)$  from diffusion, migration, and convection, respectively. Experimentally, use of sufficiently large electrolyte concentration will suppress mass transport from migration. For sufficiently slow scan rates and sufficiently fast rotation rates, steady-state mass transfer results in a time-independent current response because stirring continuously replenishes the diffusion layer with fresh material from the bulk solution. These conditions can only be achieved when voltage scans are slow relative to the time required to set up a steady-state concentration profile in the diffusion layer. This is in contrast with stationary voltammetry where the thickness of the diffusion layer increases as a function of time, leading to a time-dependent current response.

Under these conditions, the migration terms can be neglected and the RDE waveform will be described by a series of non-linear reaction-convection-diffusion equations. Recent work has shown that approximate analytical solutions can be derived using homotopy perturbation method for a limited subset of reaction mechanisms.<sup>43</sup> For reaction mechanisms where a closed-form expression does

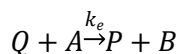
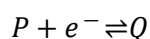


1 not exist, application of various approximations or numerical strategies can produce equations that  
2  
3 can be solved either analytically or numerically, allowing digital simulation of the current-potential  
4  
5 response at the RDE.  
6

7  
8 Using these tools, a mathematical description of the anticipated RDE waveforms have been  
9  
10 reported for a variety of homogeneous processes with coupled chemical steps.<sup>24,35,36</sup> The approaches  
11  
12 taken during this treatment can vary considerably in complexity, particularly in relation to the extent  
13  
14 of approximations used in the description of mass transfer processes.<sup>22,35,43–47</sup> Two strategies for  
15  
16 computing RDE voltammograms, pioneered by the groups of Savéant and Compton, proved  
17  
18 particularly important in developing the theory for the one-electron, one-substrate EC' catalytic  
19  
20 reaction (**Scheme 1**). In this mechanism, the one-electron reduction of substrate A to product B is  
21  
22 catalyzed by the molecular catalyst P and the rate-limiting step is the homogeneous electron transfer  
23  
24 from the reduced catalyst Q to the substrate A which proceeds with a rate constant  $k_e$ .  
25

---

### 26 **Scheme 1** EC' Reaction Mechanism



---

29  
30  
31  
32  
33  
34  
35 A general computational approach popularized by Compton and colleagues employs  
36  
37 numerical strategies derived from Hale Theory.<sup>22,48</sup> In this approach, appropriate application of the  
38  
39 Hale Transformation, which in effect applies the equivalent of a non-linear space grid, simplifies the  
40  
41 mass-transport equations by reducing the two terms corresponding to diffusion and convection into a  
42  
43 single expression. This simplification permits efficient numerical calculations of RDEV waveforms  
44  
45 without relying on gratuitous approximation in the description of mass transfer. Using this approach,  
46  
47 Compton and coworkers have described the current-potential behavior for a wide range of electrode  
48  
49 processes at the RDE,<sup>35,48–50</sup> including the EC' catalytic reaction.<sup>37,39</sup>  
50

51  
52 The second model relies on the Nernst Diffusion Layer approximation. This strategy,  
53  
54 distinguished in the works of Savéant and coworkers, assumes that the reaction kinetics are  
55  
56 sufficiently fast such that convection effects can be neglected altogether.<sup>12,38,51</sup> This approach greatly  
57  
58  
59  
60

1 simplifies the solution of the mass-transport equations as it requires that only diffusion, and not  
2 convection, be considered. It is this simplification that allows certain analytics tools used to extract  
3 rate constants from stationary cyclic voltammograms to be transposed to RDEV.<sup>52</sup>  
4  
5  
6  
7

8 One of the key differences between the two methodologies is their assumptions concerning  
9 the kinetics of the chemical step. While the Hale approach makes no assumptions about the rate  
10 constants of the chemical steps, the Nernst Diffusion Layer approach will only be accurate when  
11 reaction kinetics are sufficiently fast such that explicit consideration of convection can be neglected.  
12 Despite these differences, these two computational methodologies give consistent results when  
13 describing EC' processes across a range of conditions, with deviations only observed at very small  
14 values of  $k_e$ .<sup>37</sup> Importantly, the ability to quantitatively apply the Nernst Diffusion Layer approach is  
15 an important prerequisite for use of certain electrochemical benchmarking tools (such as plateau  
16 current analysis and foot-of-the-wave analysis, discussed further in section 2 and Supporting  
17 Information I).

## 28 **1.2 Extracting figures of merit for an EC' mechanism**

29 Under catalytic conditions, the exact shape of the waveform – and thus what, if any, metrics  
30 can be used to glean mechanistic and kinetic insight – depend (in the absence of side phenomena  
31 such as catalyst deactivation) on two factors: (1) the degree of substrate consumption at the electrode  
32 surface and (2) whether pure kinetic conditions are achieved.<sup>53</sup> These factors, in turn, depend on two  
33 dimensionless parameters, the substrate-to-catalyst excess factor ( $\gamma$ ) and the dimensionless kinetic  
34 parameter ( $\lambda$ ) (see Glossary of Symbols).<sup>14</sup> For large values of  $\gamma$  and relatively small values of  $\lambda$ , the  
35 amount of substrate consumed in the reaction diffusion layer can be considered negligible such that  
36 the concentration of substrate at the electrode surface is equal to the bulk concentration. Under these  
37 conditions, the current response will not be limited by mass transport. Pure kinetic conditions entail  
38 that the concentration profile of the two forms of the catalyst couple are confined within a thin reaction-  
39 diffusion layer that is far narrower than the diffusion layer.<sup>14</sup> This condition requires the catalytic  
40 reaction to be rapid relative to diffusion.<sup>38</sup>  
41  
42  
43  
44  
45  
46  
47  
48  
49  
50  
51  
52  
53  
54  
55  
56  
57  
58  
59  
60

1 Analytical frameworks for interpreting catalytic responses can only be rigorously applied when  
2 certain criteria related to substrate consumption and/or pure kinetic conditions are met.<sup>10</sup> Given this,  
3 it is instructive to consider what the key characteristics for RDEV waveforms are under these different  
4 limiting conditions so that they can be readily identified during analysis. We first discuss these regimes  
5 in the context of the simple EC' mechanism as a prelude to our discussion of multi-step catalytic  
6 reactions. Alongside this discussion, we will introduce relevant analytical tools for quantifying the  
7 kinetics of elementary reaction steps. While the theory and tools required to understand catalytic EC'  
8 mechanisms have long been known, the following section is one of the only modern attempts to  
9 synthesize this diverse literature into a single resource.

10  
11  
12  
13  
14  
15  
16  
17  
18  
19  
20  
21 *Case 1: Pure kinetic conditions, no substrate consumption*

22 When pure kinetic conditions are achieved with large values of  $\gamma$  and relatively small values  
23 of  $\lambda$ , substrate consumption will be negligible and the current–potential response will represent the  
24 kinetic current in the absence of mass-transfer effects (**Figure 1A**).<sup>38,54,55</sup> This steady-state catalytic  
25 response will be independent of the particular electrochemical technique – namely the same current–  
26 potential response would be obtained via RDEV and stationary CV – which allows plateau current  
27 analysis, a tool commonly employed for analysis of stationary catalytic voltammograms, to be readily  
28 extended to RDEV (**Figure 1B**).<sup>14,52</sup>

29 At this point, it is key to emphasize the difference between the steady-state response generally  
30 achieved in RDEV and the steady-state catalytic response which is uniform across all electrochemical  
31 techniques. As mentioned above, in RDEV, steady-state conditions are achieved when using  
32 sufficiently slow scan rates because stirring continuously replenishes the diffusion layer with fresh  
33 material from the bulk solution and thus all current responses reflect steady-state conditions. In  
34 contrast, steady-state is achieved under catalytic conditions when (1) rapid turnover ensures a  
35 steady-state condition in species Q such that Q does not accumulate outside of the very thin reaction-  
36 diffusion layer (pure kinetic conditions) and (2) substrate consumption is so small relative to the total  
37 substrate concentration that the substrate concentration at the electrode surface is effectively equal  
38 to the bulk concentration. This steady-state catalytic response is independent of the mode of mass

transport and thus will not vary upon changing experimental set-up, for example by moving from a stationary electrode to a RDE.

For the EC' mechanism, the observed rate constant can be directly determined from the plateau current using eq 2.<sup>10,41,56</sup>

$$i_{pl} = nFAC_P^0 \sqrt{Dk_{obs}} \quad (2)$$

Importantly, this  $i_{pl}$ - $k_{obs}$  relationship can only be used when the S-shaped current response is independent of the rotation rate (for RDEV) or scan rate (for stationary techniques).<sup>10,36</sup>

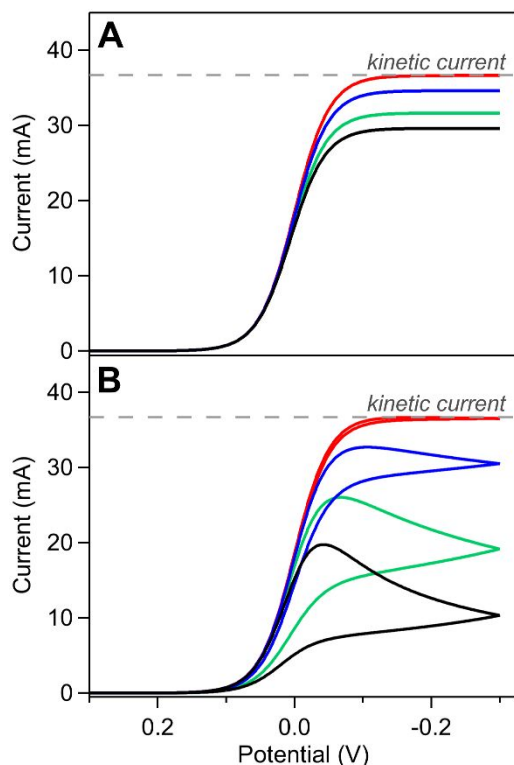


**Figure 1** Simulated voltammograms showing how the EC' catalytic waveform will approach its kinetically limited maximum – denoted in both panels by the dashed grey line – by decreasing the kinetic parameter  $\lambda$ .  $\lambda$ , which is proportional to  $\frac{k}{\omega}$  in RDEV and  $\frac{k}{v}$  in stationary CV, can be lowered by increasing rotation rate (for RDEV) or scan rate (for stationary CV) or by decreasing  $k$ . (A) RDE voltammograms collected at rotation rates of 50 (black), 100 (green), 500 (blue), and 10,000 (red)  $\text{rad s}^{-1}$ , keeping the excess factor ( $\gamma = 1000$ ,  $C_P^0 = 0.001$  M,  $C_A^0 = 1$  M) and kinetics of the chemical step ( $k_e = 3.86 \times 10^5 \text{ M}^{-1} \text{ s}^{-1}$ ) constant. For all RDE simulations, scan rate set as  $0.001 \text{ V s}^{-1}$  and kinematic viscosity set as  $0.01 \text{ cm}^2 \text{ s}^{-1}$ . (B) Analogous voltammograms collected under stationary conditions. In this case,  $\lambda$  was varied using scan rate:  $v = 0.025$  (black),  $0.1$  (green),  $1$  (blue), and

1 100 V s<sup>-1</sup> (red). The mass-transport independent plateau current is achieved at 10,000 rad s<sup>-1</sup> and 100 V s<sup>-1</sup> for  
2 RDEV and stationary CV, respectively. For all simulations, electron transfers were set at 10000 cm s<sup>-1</sup> with  $\alpha =$   
3 0.5 and diffusion coefficients of all species set as 1 x 10<sup>-5</sup> cm<sup>2</sup> s<sup>-1</sup>. Simulated using *DigiElch 8.FD*.  
4  
5  
6

---

### 8 *Case 2: Pure kinetic conditions, substrate consumption*

9

10 As  $\lambda$  grows increasingly large under pure kinetic conditions, substrate consumption can no  
11 longer be considered negligible and the concentration of substrate in the reaction-diffusion layer will  
12 be less than the bulk concentration, but still approximately constant. When this condition is met at  
13 very high values of  $\lambda$  relative to  $\gamma$ , a second limiting case of interest is reached: total catalysis.<sup>10,53,54</sup>  
14 In this regime, all substrate in the reaction diffusion layer can be consumed by the small amount of  
15 active catalyst generated at potentials positive of the catalyst's redox couple. The resulting catalytic  
16 wave is then controlled by diffusion of substrate, not diffusion of the catalyst.<sup>14</sup> This phenomenon  
17 manifests as a split of the catalytic sigmoid into two overlapping sigmoidal waves (**Figure 2**).<sup>37-39</sup> At  
18 some potential positive of the catalyst's redox couple, the onset of a catalytic wave is observed which  
19 rapidly reaches the diffusion controlled current maximum ( $\Psi^\infty = \gamma$ ). The efficiency of this catalytic  
20 process ensures that the concentration of the reduced catalyst Q is negligible relative to P due to the  
21 rapid regeneration of P via homogeneous electron transfer.<sup>37,38</sup> As the potential approaches the P/Q  
22 redox couple, reduction of P gives rise to the usual reversible redox wave of the catalyst, leading to  
23 a hybrid wave in which the typical redox couple is overlaid with the catalytic wave ( $\Psi^\infty = \gamma + 1$ ).  
24  
25  
26  
27  
28  
29  
30  
31  
32  
33  
34  
35  
36  
37  
38  
39  
40  
41  
42  
43  
44  
45  
46  
47  
48  
49  
50  
51  
52  
53  
54  
55  
56  
57  
58  
59  
60

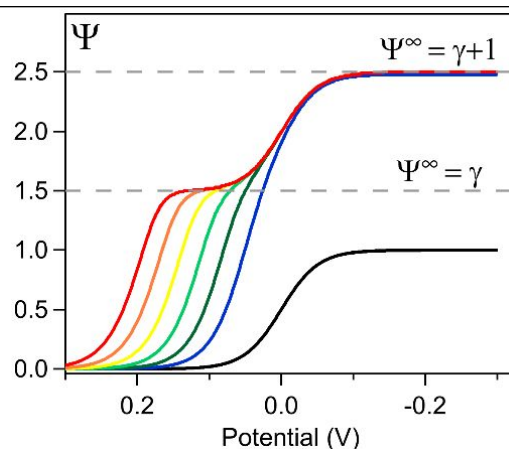


**Figure 2.** Simulated RDE voltammograms depicting how an EC' catalytic waveform varies with  $\lambda$  in the total catalysis waveforms when  $\gamma$  is constant. In the absence of substrate,  $\Psi^\infty = 1$  for the catalyst's reversible one-electron redox couple (black trace). Simulated catalytic voltammograms collected at  $\log(\lambda)$  values of 2 (blue), 3 (dark green), 4 (light green), 5 (yellow), 6 (orange), and 7 (red) for  $\gamma = 1.5$ . For all simulations, scan rate set as  $0.001 \text{ V s}^{-1}$ , kinematic viscosity set as  $0.01 \text{ cm}^2 \text{ s}^{-1}$ , electron transfers were set at  $10000 \text{ cm s}^{-1}$  with  $\alpha = 0.5$  and an  $E_{1/2}$  of  $0\text{V}$ , and diffusion coefficients of all species set as  $1 \times 10^{-5} \text{ cm}^2 \text{ s}^{-1}$ . Simulated using *DigiElch 8.FD*.

In the total catalysis regime, the plateau current is no longer a function of the catalytic rate constant, instead reflecting  $\gamma$ , and thus cannot be used to extract kinetic information. However, the catalytic rate constant will govern the location of the half-wave potential of the catalytic feature ( $\theta_{1/2}$ ) which is predicted to shift anodically by 30 mV per decade  $\lambda$  for an EC' mechanism per equation 3, while the half-wave potential for the hybrid wave is invariant and governed by the catalyst redox couple.<sup>38</sup> Rewriting equation 3 in terms of experimental parameters shows the anticipated dependence of  $E_{1/2}$  on catalyst concentration, substrate concentration, and rotation rate (equation 4).

$$\theta_{1/2} = -\left(\frac{1}{2}\right)\ln\left(\frac{2\lambda}{\gamma}\right) \quad (3)$$

$$\theta_{1/2} = -\left(\frac{1}{2}\right)\ln\left(2\frac{C_P^0}{C_A^0}\left[1.61D^{-1/6}v^{1/6}\right]^2\frac{k}{\omega}\right) \quad (4)$$

Peak shift analysis exploits this  $E_{1/2}$ - $\lambda$  relationship to derive kinetic information by tuning  $C_P^0$ ,  $C_A^0$ ,  $\omega$ , or  $k$  and tracking the subsequent change in half-wave potential relative to the half-wave potential of the catalyst couple.

1  
2 For a given  $\lambda$  value, the distinction between the two features is lost as  $\gamma$  is increased (which  
3 can be experimentally accomplished by increasing substrate concentration or decreasing catalyst  
4 concentration) and the catalytic wave continues to grow in magnitude relative to the catalyst's redox  
5 concentration) and the catalytic wave continues to grow in magnitude relative to the catalyst's redox  
6 couple. Eventually, the catalyst's redox couple will become undetectable, marking the passage of the  
7 CV response into the realm of mixed transport-kinetic control.<sup>36,38</sup> In this regime, the plateau current  
8 for the catalytic wave will be a function of both  $\lambda$  and  $\gamma$ .  
9

### 10 *Case 3: Current-potential responses outside of the pure kinetic condition*

11  
12 The situation becomes more complex when pure kinetic conditions are not met such that slow  
13 reaction kinetics result in a build-up of unreacted Q. Under stationary conditions, this behavior is  
14 easily diagnosable – an anodic feature corresponding to the oxidation of unreacted intermediates will  
15 be observed on the return scan.<sup>54,55</sup> Meanwhile, in RDEV, these intermediates will be swept out into  
16 the bulk solution where turnover can take place. At very low values of  $\lambda$  and/or  $\gamma$ , the reaction kinetics  
17 are so slow relative to rotation rate that no catalysis will be observed at the electrode surface and  
18 only the mass transport-limited, one-electron redox wave will be observed at the usual P/Q redox  
19 couple. For intermediate values of  $\gamma$ , increasing  $\lambda$  gives rise to observable catalysis at the electrode  
20 surface. In this regime, a single wave is observed which will increase in magnitude as  $\lambda$  is increased  
21 (Figure 3). At sufficiently high  $\lambda$  values, the magnitude of this feature will hit a limiting  $\Psi^\infty$  value of  $\gamma+1$   
22 which corresponds to passage into the total catalysis regime.<sup>38</sup>  
23  
24  
25  
26  
27  
28  
29  
30  
31  
32  
33  
34  
35  
36  
37  
38  
39  
40  
41  
42  
43  
44  
45  
46  
47  
48  
49  
50  
51  
52  
53  
54  
55  
56  
57  
58  
59  
60

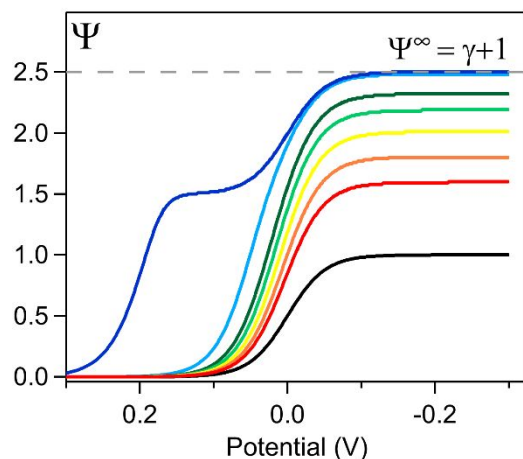


**Figure 3** Simulated RDE voltammograms for an EC' catalytic mechanism showing how slow reaction kinetics limit the plateau current at intermediate  $\gamma$  values. In the absence of substrate,  $\Psi^\infty = 1$  for the catalyst's reversible, one-electron redox couple (black trace). For  $\gamma = 1.5$ , voltammograms simulated with  $\log(\lambda) = 6$  (blue) exhibit behavior consistent with total catalysis. At the same excess factor, reduced reaction kinetics give a single feature with  $\Psi^\infty < \gamma + 1$  as shown in voltammograms simulated at  $\log(\lambda)$  values of 0.25 (red), 0.5 (orange), 0.75 (yellow), 1 (light green), and 1.25 (dark green). The transition to total catalysis can be observed at  $\log(\lambda) = 2$  (light blue). For all simulations, scan rate set as  $0.001 \text{ V s}^{-1}$ , kinematic viscosity set as  $0.01 \text{ cm}^2 \text{ s}^{-1}$ , electron transfers were set at  $10000 \text{ cm s}^{-1}$  with  $\alpha = 0.5$ , and diffusion coefficients of all species set as  $1 \times 10^{-5} \text{ cm}^2 \text{ s}^{-1}$ . Simulated using *DigiElch 8.FD*.

### 1.3 Mathematical modelling for a multi-step mechanism

Recent advances in digital simulation software allow the hydrodynamic response of practically any electrochemical mechanism involving the coupling of heterogeneous electron transfer and homogeneous chemical reactions to be generated. These powerful and convenient tools are incredibly useful when differentiating between different mechanistic pathways, when testing whether derived analytical equations can be empirically extended to new mechanisms and catalytic waveforms, or simply as means of easily generating figures which convey important or complex concepts (as shown extensively in this work).<sup>16,42,53,57,58</sup> Despite their utility, these tools cannot replace a mathematical model that identifies the minimal number of governing dimensionless parameters. It is this rigorous mathematical treatment that allows conclusive identification of the important



1 experimental parameters (ex. catalyst concentration, rotation rate, etc.) that influence the  
2 electrochemical response – information that is crucial for intelligently designing experiments – and  
3 derivation of generalized quantitative expressions for retrieving kinetic information from current  
4 responses.  
5  
6  
7  
8  
9

10 When building models for two-electron, two-step homogeneous molecular catalysts, the operative  
11 reaction mechanism(s) must be carefully considered.<sup>16,17,52,59</sup> During mechanistic analysis, a number  
12 of questions must be answered:  
13  
14

15 (1) Is the process homolytic or heterolytic?

16 (2) What is the relative sequence of electron transfer steps and chemical steps (C)? Do the  
17 electron transfer steps occur at the electrode (E) or in solution (E')?  
18  
19

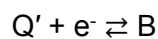
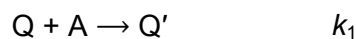
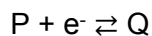
20 (3) What is the rate-limiting chemical step?

21 (4) Is the first or second electron transfer more thermodynamically difficult?  
22  
23  
24

25 It is beyond the scope of this paper to consider all permutations available for multi-step  
26 catalytic reactions. Instead, this paper builds RDEV models pertinent to an ECEC' reaction  
27 mechanism (Scheme 2) where the second electron transfer is more thermodynamically favorable  
28 than the first and the first chemical step is not rate-limiting. The motivation for focusing on the ECEC'  
29 reaction mechanism are two-fold: (1) it is one of the most commonly invoked mechanistic pathways  
30 for two-step catalytic processes and (2) it is pertinent to the model complex used to experimentally  
31 test this theoretically work (see section 2.1).<sup>42</sup> Despite the specificity of this report, we hope the  
32 following discussion along with the detailed derivations in Supporting Information 1 will provide a solid  
33 framework which readers can extend to other multielectron, multistep molecular catalytic processes.  
34  
35  
36  
37  
38  
39  
40  
41  
42  
43  
44  
45

---

46 **Scheme 2** ECEC' Reaction Mechanism



1  
2 Assuming the electrolyte concentration is sufficiently large to suppress mass transport from  
3 migration, RDE waveforms for an ECEC' process will be described by a system of six non-linear  
4 reaction-convection-diffusion equations whose solutions have no closed form. Two mathematical  
5 models based on the Hale approach and Nernst Diffusion Layer approach were used to approximate  
6 the relevant solutions and generate two mathematical models describing the current–potential  
7 behavior of the homogeneous ECEC' mechanism at the RDE.<sup>12,35</sup> Digital simulations based on both  
8 models were carried out using a custom MATLAB script that implemented finite difference-based  
9 approximations to these models. To test the validity of these models, the current-potential behavior  
10 for a reversible electron transfer was calculated.<sup>60</sup> In both cases, mass transport-corrected Tafel plots  
11 of  $\theta$  vs  $\log(i^{-1} - i_{pl}^{-1})$  had the requisite slope of 2.303, supporting the use of these numerical  
12 approaches (SI-2, Supporting Information 2).<sup>61</sup>

13  
14 The following discussion focuses on the conclusions that can be draw from these digital  
15 simulations instead of the derivations themselves. The current-potential curves predicted by the  
16 Nernst Diffusion Layer and Hale approach are compared under a variety of limiting conditions in order  
17 to identify conditions in which the more minimalist Nernst Diffusion Layer approach may be applied.  
18 The parameters that govern the behavior of these voltammetric responses are identified and  
19 discussed. Readers interested in a detailed discussion of these derivations and MATLAB scripts for  
20 simulating ECEC' RDE responses are directed to SI-1 and SI-2, Supporting Information I.

### 21 *1.3.1 Current-potential behavior calculated by the Nernst Diffusion Layer and Hale approach*

22  
23 Initial simulations explored the current–potential behavior calculated by the two models under  
24 pure kinetic conditions when both electrode electron transfers are Nernstian. Under pure kinetic  
25 conditions, two limiting regimes exist depending on the magnitude of the excess factor. The first  
26 limiting case occurs when substrate consumption is negligible and the voltammogram provides the  
27 kinetic current in the absence of mass transfer effects. In this regime, the catalytic responses derived  
28 from the two approaches converge and the dimensionless current value for these responses show

1 the anticipated dependence on the rate constant for the rate limiting step (SI-3, Supporting  
2 Information I).  
3  
4

5  
6 The second limiting regime occurs at small values of  $\gamma$  where complete consumption of the  
7 substrate in the reaction diffusion layer results in a catalytic wave controlled by substrate diffusion. In  
8 this case, both simulation procedures yield “split wave” voltammograms in which two distinct features  
9 can be resolved: (1) a catalytic wave at potentials positive of the catalyst’s redox couple followed by  
10 (2) the typical reversible redox wave of the catalyst which have  $\Psi^\infty$  values of  $\gamma$  and  $\gamma+1$ , respectively  
11  
12  
13  
14  
15  
16  
17  
18  
19  
20  
21  
22  
23  
24  
25  
26  
27  
28  
29  
30  
31  
32  
33  
34  
35  
36  
37  
38  
39  
40  
41  
42  
43  
44  
45  
46  
47  
48  
49  
50  
51  
52  
53  
54  
55  
56  
57  
58  
59  
60

To qualitatively test the robustness of the Nernst Diffusion Layer and Hale-based modelling procedures, a series of simulated voltammograms in the total catalysis regime were generated. Then  $\gamma$  or  $\lambda$  were systematically modulated. Monitoring the changes in the shape of these waveform as a function of these two parameters provides a qualitative means to ensure that these modelling procedures produce voltammograms that follow chemically intuitive trends.<sup>55</sup> For all of these simulations, both methods generate convergent voltammograms. First,  $\gamma$  was modulated at a constant value of  $\lambda$  in the pure kinetic regime. As described above, low  $\gamma$  values result in split wave voltammograms consistent with total catalysis. Upon increasing  $\gamma$  at a constant value of  $\lambda$ , the distinction between these features is lost as the catalytic wave grows in magnitude relative to the catalyst’s redox couple, consistent with the expected transition to mixed transport-kinetic control (Figure S4, Supporting Information I). If  $\gamma$  is pushed to even larger values, the observed current approaches the kinetically limited current in the absence of mass transport effects, as anticipated for a system under pure kinetic conditions. Next,  $\lambda$  was modulated at a constant value of  $\gamma$ . Starting in the total catalysis regime, decreasing  $\lambda$  results in a smooth transition from total catalysis to no detectable catalysis, as expected for voltammograms that are not under pure kinetic conditions (Figure 4).

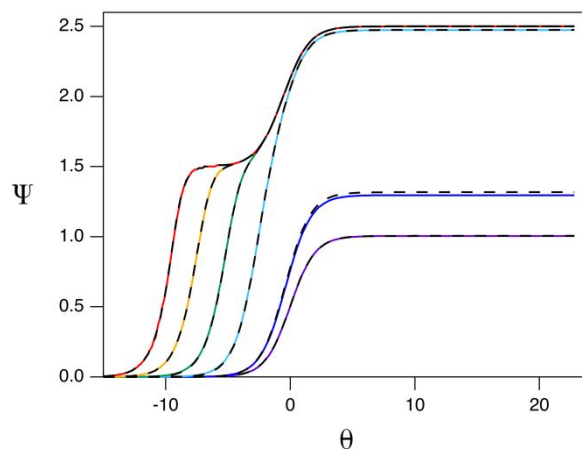


**Figure 4** Simulated RDE voltammograms for an ECEC' catalytic mechanism utilizing the Hale transformation approach (dotted lines) and the Nernst Diffusion Layer approximation approach (solid lines). Here  $\gamma = 1.5$ , and dimensionless rate parameters for both models were equated. Voltammograms were collected at  $\log(\lambda)$  values of 8 (dark red), 6 (light orange), 4 (green), 2 (light blue), 0 (dark blue), and -2 (dark purple) corresponding to the transition between no observed catalysis to total catalysis when  $\Psi^\infty = \gamma + 1$ . Simulations generated using custom MATLAB scripts.

To investigate the possible impact of electron transfer kinetics on the shape and cathodic shift of the catalytic voltammogram for an ECEC' mechanism, the mathematical models were modified by substituting Butler Volmer boundary conditions for the typical Nernstian boundary at the electrode surface and simulations were obtained in the total catalysis regime. For voltammograms in this regime, decreasing the rate constant of heterogeneous electron transfer leads to a negative potential shift in the half-wave potential of the catalytic wave (**Figure 5**). When electron transfer deviates sufficiently from the Nernstian regime, the splitting of the two waves vanishes and a single curve is observed.

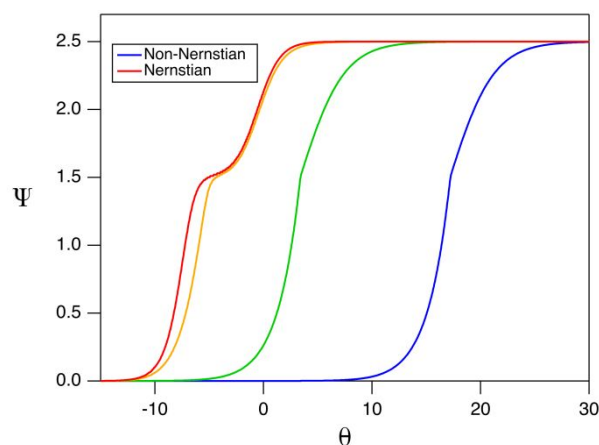


**Figure 5** Simulated ECEC' RDE waveforms displaying the effects of electron transfer kinetics on both the shape and cathodic shift in the total catalysis regime. Split-wave voltammograms are observed in simulations modelling Nernstian electron transfer kinetics (red,  $\log[k_s] = 3$ ), as anticipated for a voltammogram in the total catalysis regime. As electron transfer kinetics become increasingly slow, the distinction between the split waves is lost and the potential for the features shifts cathodically. RDE voltammograms depicting non-Nernstian electron transfer collected with  $\log(k_s)$  values of -6 (blue), -3 (green), and -1 (orange). The excess parameter,  $\gamma$ , was set to 1.5 and  $\log(\lambda)$  for both chemical steps set to 7 to simulate total catalysis. Simulations generated using custom MATLAB scripts.

Under all conditions explored, both formulations towards modeling yield catalytic voltammograms that show excellent qualitative agreement in the general shape of the waveform as well as quantitative agreement with each other in the plateau current magnitudes – which deviate only by 1.3% when the reaction kinetics are slow – and the half-wave potentials (**Figure 4** and SI-3, Supporting Information I). Convergence of these simulation methods supports quantitative use of the more simplified Nernst Diffusion Layer approach across the conditions explored.

### 1.3.2 Governing parameters for an ECEC' process

Derivation of the general expression for an ECEC' mechanism (Scheme 2) allows parameters governing the current-potential response to be identified (SI-1, Supporting Information I). For multi-step catalytic reactions where only a single type of substrate participates in the reaction, such as proton reduction catalysis, a single excess factor is operative. Two dimensionless kinetic parameters

$\lambda_1 = (\delta/\mu_1)^2$  and  $\lambda_2 = (\delta/\mu_2)^2$  are now necessary to account for the competition between the two chemical reactions described by rate constants  $k_1$  and  $k_2$ , along with diffusion.

For a system under pure kinetic conditions with negligible substrate consumption and Nernstian electron transfer, the plateau current will be governed by  $\gamma$  and the kinetic parameter for the rate-limiting step ( $\lambda_2$  in the mechanism considered here). Outside of the plateau current, the shape of the voltammogram is also governed by the ratios of the rate constants for the two chemical steps ( $k_1/k_2$ ) as well as the potential separation between both electron transfer steps ( $\Delta E = E_2 - E_1$ ) (**Figure 6**). These additional thermodynamic and kinetic parameters can greatly influence the accuracy of analytical methods applied to extract figures of merit from these regions and thus should be carefully considered to avoid potential errors (see section 2.3.2).<sup>16</sup>

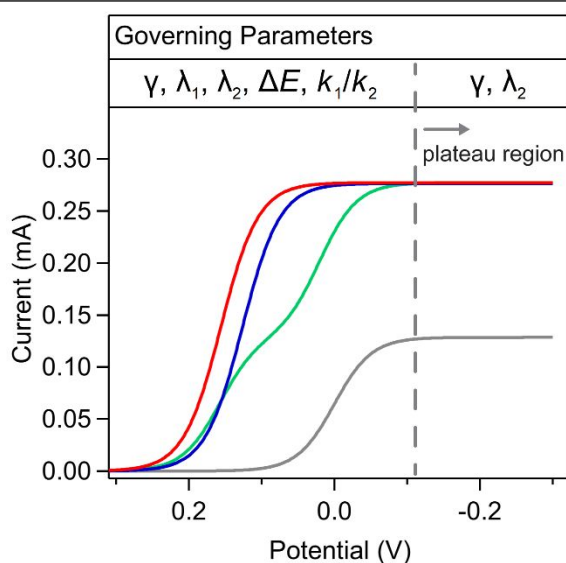


**Figure 6** Simulated RDE voltammograms illustrating parameters that govern the shape of the voltammogram for an ECEC' catalytic reaction where the second electron transfer is more thermodynamically favorable, the first chemical step is not rate limiting, and Nernstian electron transfer kinetics are operative. Simulated voltammogram for the one-electron redox couple of the catalyst ( $E_{1/2} = 0$  V) in the absence of substrate shown in grey. Catalytic RDE voltammograms show that changing the potential difference between  $E_1$  and  $E_2$ , the  $k_1/k_2$  ratio, and/or  $\lambda_1$  while keeping  $\gamma$  ( $C_P^0 = 0.001$  M;  $C_A^0 = 0.1$  M) and  $\lambda_2$  constant ( $k_2 = 10$  M s<sup>-1</sup>;  $\omega = 100$  rad sec<sup>-1</sup>) leads to drastic deviations in the shape of the catalytic wave *at potentials positive of the plateau region*. The values for  $k_1/k_2$  and  $\lambda_1$  were varied at a constant  $\Delta E$  value ( $E_1 = 0$  V;  $E_2 = 0.4$  V) by modulating  $k_1$  from  $1 \times 10^7$

1 M<sup>-1</sup> s<sup>-1</sup> (red) to 1x10<sup>6</sup> M<sup>-1</sup> s<sup>-1</sup> (blue). Alternatively,  $k_1/k_2$  and  $\lambda_1$  value were kept constant ( $k_1 = 1 \times 10^7$  M<sup>-1</sup> s<sup>-1</sup>) and  
2  
3  $\Delta E$  was modulated by changing  $E_2$  from 0.4 (red) to 0.02 V (green) while maintaining a constant  $E_1$  ( $E_1 = 0$  V).  
4  
5 The dashed grey line denotes the start of the plateau region where all three catalytic voltammograms display  
6  
7 the same limiting current value. The plateau current is governed by the kinetic parameter for the rate-limiting  
8  
9 step  $\lambda_2$  and excess factor  $\gamma$ . At potentials positive of the plateau region, three additional parameters influence  
10  
11 the waveform: the kinetic parameter for the first chemical step ( $\lambda_1$ ), the difference in formal potential for electron  
12  
13 transfer steps ( $\Delta E$ ), and the ratio of the rate constants for the chemical steps ( $k_1/k_2$ ). Electron transfers were  
14  
15 set at  $k_S = 1 \times 10^5$  cm s<sup>-1</sup> with  $\alpha = 0.5$ , respectively, scan rate as 0.001 V s<sup>-1</sup>, diffusion coefficients of all species  
16  
17 as 1x10<sup>-5</sup> cm<sup>2</sup> s<sup>-1</sup>, and kinematic viscosity as 0.0045 cm<sup>2</sup> s<sup>-1</sup>. Simulated using *DigiElch 8.FD*.  
18

---

19  
20 If non-Nernstian electron transfer is operative, the role of interfacial electron transfer must also  
21  
22 be considered. The convoluting role of interfacial electron transfer is clearly illustrated in Figure 5  
23  
24 which shows the sensitivity of the  $E_{1/2}$  of the catalytic wave in the total catalysis regime to changes in  
25  
26  $k_S$ . Importantly, these deviations can already be observed at  $k_S$  values pertinent to many molecular  
27  
28 fuel-forming catalysts. One characteristic of these simulations worth highlighting is that even though  
29  
30  $k_S$  influences the potential at which the full wave plateau current is reached, all simulations eventually  
31  
32 plateau at the  $\Psi_\infty = \gamma + 1$  value expected for voltammograms in the total catalysis regime once  
33  
34 sufficiently negative potentials are reached. This behavior will hold true for any system with slow  
35  
36 interfacial electron transfer and stems from the fact that heterogeneous electron transfer, not the  
37  
38 homogenous reaction kinetics, is rate limiting.  
39

### 40 41 1.3.3 Additional considerations for multistep processes – Incomplete catalysis

42  
43 For EC' reactions with slow reaction kinetics for the homogeneous chemical step, the reduced  
44  
45 catalyst may be swept away from the electrode surface before catalytic turnover, resulting in no  
46  
47 observable catalytic current. We postulated that for multi-step reactions judicious choice of reaction  
48  
49 conditions could allow catalytic turnover to be outcompeted and different steps along the ECEC'  
50  
51 reaction pathway isolated, leading to “intermediate” zones which would reflect (depending on the  
52  
53 relative kinetics of the different chemical steps) simply the initial EC or ECE steps in the absence of  
54  
55 turnover. Our interest in seeing if these intermediate zones can be isolated is two-fold. For one, it  
56  
57

1 would provide a more general means of identifying catalytic mechanisms through isolation of  
2 elementary steps. Second, these limiting regimes are expected to exhibit characteristic changes in  
3 waveform properties (ex.  $E_{1/2}$ ) upon tuning experimental parameters, relationships that could allow  
4 kinetic information to be determined. Work detailing these types of relationships for EC and ECE  
5 reaction schemes have been reported; however, the chemical steps modeled in these works were  
6 either unimolecular or bimolecular dimerization, making it far more simple to derive  $E_{1/2}$ - $\lambda$  relationships  
7 for the reaction schemes than it will be for elementary steps operative in catalytic mechanisms  
8 relevant to fuel-forming reactions. While this limited scope restricts their direct use, it does not  
9 preclude extension of these equations to the more complex reactions as a future avenue for  
10 exploration – albeit one that will not be discussed in this work.

22 For the ECEC' catalytic mechanism described in Scheme 1, three limiting behaviors exist.

- 23 (1) E Mechanism: Electron transfer from the electrode will generate the singly reduced catalyst  
24 Q, however the first chemical step will not take place at the electrode surface. Only the mass-  
25 transport limited redox wave will be observed at the usual P/Q redox couple.  
26  
27 (2) EC Mechanism: If the first chemical step is observable on an experimentally relevant  
28 timescale while the second electron transfer is slow relative to rotation rate, the product of the  
29 EC reaction Q' will be swept into the bulk solution. A single peak will be observed in the RDE  
30 voltammogram with a plateau current identical to that observed for the P/Q redox couple in  
31 the absence of substrate ( $\Psi^\infty = 1$ ). For a EC reaction scheme, theory shows that the follow-  
32 up chemical reaction will result in a positive shift of ca. 30 mV  $(\log_{10}\omega)^{-1}$  in the half-wave  
33 potential of this feature for a unimolecular first order reaction and a ca 20 mV  $(\log_{10}\omega)^{-1}$  shift  
34 for a second order, bimolecular dimerization.<sup>24,35,49</sup> A dependence of the half-wave potential  
35 on rotation rate is anticipated if the EC elementary steps operative in the ECEC' mechanism  
36 can be isolated, however the specific  $E_{1/2}$ - $\lambda$  relationship will likely vary because the  
37 bimolecular EC mechanism involves a reaction between two different substrates.

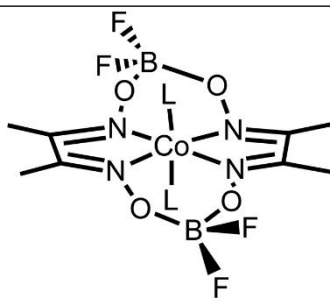


1  
2 (3) ECE Mechanism: When the second chemical step is slow relative rotation rate, the current-  
3  
4 potential response for an ECE reaction will be observed which will manifest as a single wave  
5  
6 with  $\Psi^\infty = 2$  as well as a positive shift in  $E_{1/2}$ .<sup>24,35</sup>  
7

8 Obtaining waveforms with  $\Psi^\infty > 2$  indicates that at least some turnover is occurring, regenerating P  
9  
10 which is then further reduced at the electrode surface. While the broad diagnostic criteria outlined  
11  
12 above are helpful for visualizing what parameters can be analyzed to glean mechanistic insight,  
13  
14 completely isolating only a single limiting regime is only likely to happen under extreme conditions.  
15  
16 However, the transition between these zones can still provide important insight into the competition  
17  
18 between limiting steps as well as the relative order of the chemical and electron transfer steps for an  
19  
20 unknown mechanism.  
21  
22  
23  
24  
25  
26  
27  
28  
29  
30  
31  
32  
33  
34  
35  
36  
37  
38  
39  
40  
41  
42  
43  
44  
45  
46  
47  
48  
49  
50  
51  
52  
53  
54  
55  
56  
57  
58  
59  
60

## 2. Experimental analysis of a HER electrocatalyst by RDEV

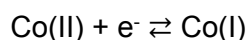
To experimentally validate the extension of RDEV to homogeneous ECEC' reactions, RDE techniques were applied to a well-studied cobaloxime HER electrocatalyst. Cobaloxime derivatives are a popular class of proton reduction catalysts due to their versatility in HER systems.<sup>62</sup> Active under both aqueous and nonaqueous conditions, their operative catalytic mechanism(s) have been the subject of extensive experimental and theoretical investigation.<sup>42,62–70</sup> RDEV has been previously used to compare the catalytic activity for a series of cobaloxime catalysts under aqueous conditions, however no theoretical treatment of homogeneous, multi-step catalytic processes at the RDE or additional kinetic and mechanistic analysis were reported as part of this study.<sup>33</sup> Kinetic analysis of HER by the cobaloxime electrocatalyst  $\text{Co}(\text{dmgBF}_2)_2(\text{CH}_3\text{CN})_2$  ( $\text{dmgBF}_2$  = difluoroboryl-dimethylglyoxime) (**Figure 7**) in organic solvents with *para*-substituted anilinium acids has been conducted by our group using stationary CV.<sup>42,55</sup> We reasoned that revisiting this well-characterized catalyst would provide a means of validating the theoretical treatment derived in part 1 while also allowing direct comparison of stationary CV and RDEV as tools for evaluating homogeneous HER electrocatalysts.

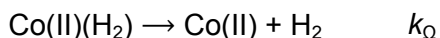
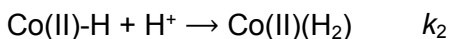
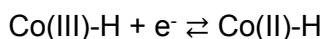


**Figure 7** Structure of  $\text{Co}(\text{dmgBF}_2)_2(\text{L})_2$  HER electrocatalyst.

### 2.1 Mechanism of $\text{H}_2$ production by $\text{Co}(\text{dmgBF}_2)_2(\text{CH}_3\text{CN})_2$

The ECEC' HER pathway for  $\text{Co}(\text{dmgBF}_2)_2(\text{CH}_3\text{CN})_2$  in acetonitrile when using *para*-substituted anilinium acids as the proton source can be summarized as follows:





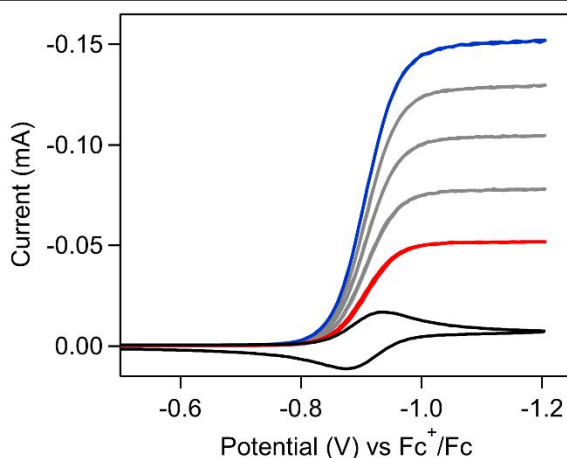
This pathway contains three chemical steps: (1) protonation of the singly reduced Co(I) species to generate Co(III)-H (rate constant  $k_1$ ), (2) protonation of the reduced cobalt hydride Co(II)-H to generate Co(II)(H<sub>2</sub>) (rate constant  $k_2$ ), and (3) a final acid-independent step involving H-H bond formation or H<sub>2</sub> release (rate constant  $k_{\Omega}$ ). For all acids employed, the first protonation is rapid. While  $k_2$  is rate limiting under most conditions,  $k_{\Omega}$  becomes limiting for strong acids at high substrate concentrations.

Computational studies concluded that the second electron transfer is more facile than the first, with the reduction potential of Co(III)-H estimated to be 20-100 mV more positive than the Co<sup>III/I</sup> couple.<sup>67,70</sup> Stationary electrochemistry furnished no evidence for homogeneous electron transfer from Co(I) to Co(III)-H through a solution electron transfer mechanism. These results are consistent with the relatively slow rate constant independently determined for this homogeneous electron transfer ( $k = 9.2 \times 10^6 \text{ M}^{-1} \text{ s}^{-1}$ ) and indicate that the two electrons required to complete catalytic turnover are transferred to the catalyst from the electrode.<sup>69</sup> We anticipate that the dominate reaction mechanism will remain the same within the confines of the reaction-diffusion layer, though divergent behavior may occur in the bulk solution if reactive intermediates are swept into solution before completing the catalytic cycle.

## 2.2 Electrochemistry of Co(dmgbF<sub>2</sub>)<sub>2</sub>(CH<sub>3</sub>CN)<sub>2</sub>

During electrochemical trials, Co(dmgbF<sub>2</sub>)<sub>2</sub>(CH<sub>3</sub>CN)<sub>2</sub> is generated upon dissolving Co(dmgbF<sub>2</sub>)<sub>2</sub>(H<sub>2</sub>O)<sub>2</sub> in acetonitrile. In the absence of acid, RDE voltammograms of Co(dmgbF<sub>2</sub>)<sub>2</sub>(CH<sub>3</sub>CN)<sub>2</sub> contain a reversible reductive wave with a half-wave potential of -0.91 V (all values reported vs Fc<sup>+0</sup> couple) assigned to the Co<sup>III/I</sup> couple (**Figure 8**). The plateau current for this feature varies linearly with  $\omega^{1/2}$ , allowing a diffusion coefficient (D) to be extracted per the Levich equation (SI-1, Supporting Information II).<sup>12</sup> This diffusion coefficient ( $D = 9.15 \times 10^{-6} \text{ cm}^2 \text{ s}^{-1}$ ) is in

1 good agreement with values obtained from stationary voltammetry ( $D = 9.22 \times 10^{-6} \text{ cm}^2 \text{ s}^{-1}$ ). Deviations  
2 from the idealized sigmoidal waveshape occurred at high rotation rates ( $\omega \geq 377 \text{ rad s}^{-1}$ ), consistent  
3 with kinetic limitations imposed by the electron transfer process.<sup>12</sup>  
4  
5  
6



7  
8  
9  
10  
11  
12  
13  
14  
15  
16  
17  
18  
19  
20  
21  
22  
23 **Figure 8** Stationary cyclic voltammogram (black) and RDE voltammograms of 0.5 mM  $\text{Co}(\text{dmgbF}_2)_2(\text{CH}_3\text{CN})_2$   
24 in 0.25 M  $[\text{NBu}_4][\text{PF}_6]$  acetonitrile solution at 0.025 and 0.01  $\text{V s}^{-1}$ , respectively. Rotation rates for RDE  
25 voltammograms range from 42  $\text{rad sec}^{-1}$  (red) to 377  $\text{rad sec}^{-1}$  (blue).  
26  
27  
28

### 29 30 **2.3 Electrochemistry of $\text{Co}(\text{dmgbF}_2)_2(\text{CH}_3\text{CN})_2$ in the presence of acid**

31  
32 Voltammetric responses for  $\text{Co}(\text{dmgbF}_2)_2(\text{CH}_3\text{CN})_2$  were recorded in the presence of three  
33 acids spanning 2.6  $\text{p}K_a$  units [ $\text{p}K_a(\text{CH}_3\text{CN})$ : 4-methoxyanilinium  $\text{p}K_a = 11.86$ ;<sup>71</sup> anilinium,  $\text{p}K_a =$   
34 10.62;<sup>71</sup> 4-trifluoromethoxyanilinium,  $\text{p}K_a = 9.28$ <sup>42</sup>]. In all trials, addition of acid led to current  
35 enhancement near  $E^{0'}(\text{Co}^{\text{III/I}})$ . The degree of current enhancement increased upon moving to lower  
36  $\text{p}K_a$  acids or higher acid concentrations, as expected for a catalytic wave (Table 1, **Figure 9**, and SI-  
37 2, Supporting Information II). In all cases, the  $E_{1/2}$  for the catalytic wave was positive of the  $\text{Co}^{\text{III/I}}$   
38 couple, behavior consistent with a catalytic pathway where the first chemical step is rapid relative to  
39 subsequent chemical steps.  
40  
41  
42  
43  
44  
45  
46  
47  
48  
49  
50  
51  
52  
53  
54  
55  
56  
57  
58  
59  
60

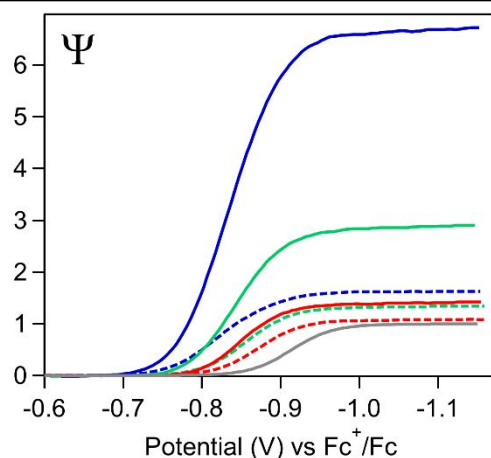


**Figure 9** RDE voltammograms of 0.5 mM  $Co(dmgBF_2)_2(CH_3CN)_2$  in the absence of acid (grey) and in the presence of 0.5 mM (dashed lines) or 5 mM (solid lines) 4-trifluoromethoxyanilinium (blue), anilinium (green), and 4-methoxyanilinium (red) illustrate how the degree of current enhance increases with stronger acids and higher acid concentrations. In all cases, the catalytic wave falls at potentials positive of the  $Co^{III}$  redox couple. All voltammograms obtained in 0.25 M  $[NBu_4][PF_6]$  acetonitrile at  $0.01\text{ V s}^{-1}$  and recorded at  $42\text{ rad sec}^{-1}$ . The vertical axis has been converted to dimensionless current.

Acid  $pK_a$  also influences the relationship between the catalytic plateau current ( $i_{pl}$ ) and acid concentration. A first-order dependence of  $i_{pl}$  on  $(\text{acid concentration})^{1/2}$  was observed for anilinium, indicating that the observed rate constant for catalysis is first order in acid. In contrast, a linear relationship between  $i_{pl}$  and acid concentration with a slope of  $-0.3\text{ mA cm}^{-2}\text{ M}^{-1}$  was observed for 4-trifluoromethoxyanilinium, indicating that the catalytic response is governed by diffusion of substrate into the reaction layer (SI-2, Supporting Information II).<sup>14</sup> These  $i_{pl}$ –acid concentration relationships are consistent with those observed during stationary electrochemical trials.<sup>42,65,66,72</sup>

In some trials, the current response deviated from the sigmoidal shape expected under steady state conditions. Instead of reaching the flat, potential-independent plateau current expected for a steady-state voltammogram, these catalytic responses exhibited a sloping plateau which did not reach a limiting value within the experimental potential window. Possible phenomena underpinning this failure to obtain a flat plateau are discussed in more detail in section 3.3 and the methodology used to identify a limiting current value for these non-ideal cases are described in SI-2, Supporting

Information II. While these challenges introduce quantitative uncertainty in some analysis, they do not impact the overarching qualitative trends.

### 2.3.1 Qualitative trends upon varying acid $pK_a$ , acid concentration, and rotation rate

Variable rotation rate studies were conducted for 0.5 mM  $\text{Co}(\text{dmgBF}_2)_2(\text{CH}_3\text{CN})_2$  in the presence of 1 and 10 equivalents of each acid in order to qualitatively explore the competition between kinetics and mass transport (Table 1, Figure 10, and SI-2, Supporting Information II). It should be noted that each set of variable rotation rate trials was collected with the same working electrode without polishing between RDE voltammograms and in the same solution of  $\text{Co}(\text{dmgBF}_2)_2(\text{CH}_3\text{CN})_2$  and acid. As rotation rates were sampled in ascending order, this introduces quantitative error which will become more acute at higher rotation rates due to the confounding factors detailed in Part 3. Despite this quantitative uncertainty, the qualitative trends will still be pertinent, especially those observed at low rotation rates.

**Table 1**  $\Psi^\infty$  values for variable rotation rate studies (42 – 262 rad  $\text{sec}^{-1}$ )

acid	$\gamma$	$\Psi^\infty$ (262 – 42 rad $\text{sec}^{-1}$ )
4-trifluoromethoxyanilinium ( $pK_a = 9.28$ )	1	1.62-1.65
	10	5.23-6.74
anilinium ( $pK_a = 10.62$ )	1	1.27-1.36
	10	2.6-2.9
4-methoxyanilinium ( $pK_a = 11.86$ )	1	1.04-1.09
	10	1.39-1.41

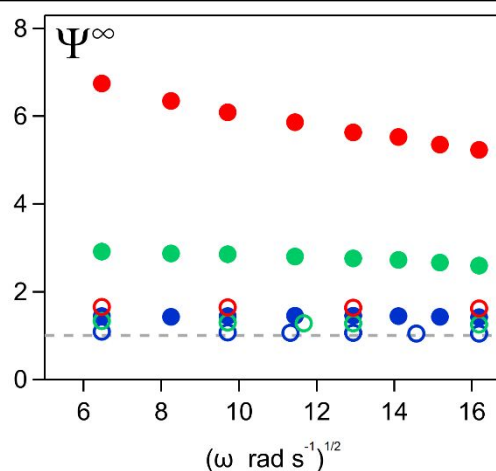


**Figure 10** Variation in  $\Psi^\infty$  as a function of rotation rate for RDE voltammograms of 0.5 mM  $\text{Co}(\text{dmgbF}_2)_2(\text{CH}_3\text{CN})_2$  in the presence of either 0.5 (hollow circles) or 5 (solid circles) mM 4-methoxyanilinium (blue), anilinium (green), and 4-trifluoromethoxyanilinium (red). Dashed grey line represents  $\Psi^\infty$  for 0.5 mM  $\text{Co}(\text{dmgbF}_2)_2(\text{CH}_3\text{CN})_2$  in the absence of substrate. Voltammograms recorded at  $0.01 \text{ V sec}^{-1}$  in  $0.25 \text{ M} [\text{NBu}_4][\text{PF}_6]$  acetonitrile. Rotation rates varied from  $42\text{-}262 \text{ rad sec}^{-1}$  in ascending order. All  $\Psi^\infty$  values calculated using the baseline corrected catalytic plateau currents. See SI-2, Supporting Information II for RDE voltammograms and further information on experimental parameters.

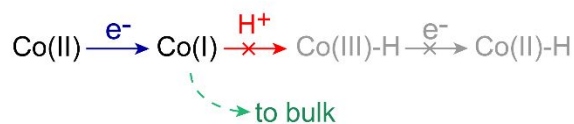
In the presence of 10 equivalents of 4-trifluoromethoxyanilinium and anilinium,  $\Psi^\infty$  values greater than 2 were obtained at all rotation rates, implying catalyst turnover occurs at the electrode surface. As the rotation rate was increased over a range of  $42\text{-}262 \text{ rad sec}^{-1}$ ,  $\Psi^\infty$  monotonically decreased by 1.5 and 0.3 units for 4-trifluoromethoxyanilinium and anilinium, respectively. The dependence of  $\Psi^\infty$  on rotation rate indicates that the catalytic response is under mixed mass transport-kinetic control. In contrast, a  $\Psi^\infty$  value of approximately 1.4 was observed at all rotation rates for voltammograms recorded in the presence of 10 equivalents of the weaker acid 4-methoxyanilinium, indicating catalyst turnover does not take place at the electrode surface.

A peak current in the range of  $1 < \Psi^\infty < 2$  indicates that some percentage of catalyst at the electrode surface undergoes the ECE portion of the catalytic cycle before being swept into the bulk solution, however the fate of the remaining fraction of catalytic species at the electrode surface as well as what limiting elementary step hinders their ability to undergo a complete ECE conversion

remains unclear. Namely, while this peak current range implies a single electron transfer from the electrode to this remaining fraction of catalytic species does take place, it provides no information as to whether these singly reduced species are protonated at the electrode surface. One possibility is that the current is limited solely by the kinetics of the first protonation ( $k_1$ ) (**Figure 11**, Pathway A). In this scenario, fast electrode kinetics ensure that all EC products generated at the electrode surface are immediately reduced, however the rate of protonation is so slow that only a fraction of the singly reduced Co(I) at the electrode surface are protonated and thus available to undergo a second electron transfer. The second extreme is that sluggish kinetics for the second electron transfer limit the current response (**Figure 11**, Pathway B). In this scenario, a rapid initial protonation coupled with slow interfacial charge transfer to the Co(III)-H species leads to a build-up of EC products at the electrode surface, only a small portion of which are reduced before being swept into solution. The latter explanation is in line with qualitative observations from stationary electrochemical analysis; an anodic feature corresponding to the oxidation of Co(III)-H is observed in stationary cyclic voltammograms when working with weak acids such as 4-methoxyanilinium.<sup>55</sup>

---

**Pathway A.**  $k_1$  limiting



**Pathway B.**  $E_2$  limiting

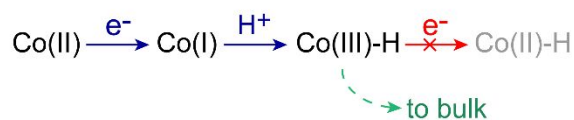


**Figure 11** Two limiting scenarios will result in catalytic voltammograms with plateau current values of  $1 < \Psi^\infty < 2$ . (A) If the kinetics for the first protonation step ( $k_1$ ) are slow relative to rotation rate, the singly reduced Co(I) species will be swept away from the electrode surface before protonation can occur. This limits the amount of EC product Co(III)-H available for reduction at the electrode surface. (B) Alternatively, the current may be limited by the rate of electron transfer from the electrode to the EC product Co(III)-H. In this case, only a fraction of the Co(III)-H is reduced at the electrode surface before being swept into the bulk solution.



1  
2  
3  
4 Upon moving to 1 equivalent of acid,  $\Psi^\infty$  values less than 2 are obtained for all acids at all  
5 rotation rates sampled. The two strongest acids show a far smaller variance of  $\Psi^\infty$  as a function of  
6 rotation rate with  $\Psi^\infty$  values of ca. 1.6 and 1.3 observed at all rotation rates for 4-  
7 trifluoromethoxyanilinium and anilinium, respectively. The magnitude of these  $\Psi^\infty$  values are  
8 consistent with a transition between the EC and ECE regimes. For 4-methoxyanilinium, a single peak  
9 with a  $\Psi^\infty$  near 1 was observed indicating there is little to no contribution to the current from the  
10 second electron transfer. However, even at the fastest rotation rate, the half-wave potential of this  
11 feature falls nearly 30 mV positive of the  $\text{Co}^{\text{III}}$  redox couple (**Figure 13**). This large positive shift in  $E_{1/2}$   
12 coupled with a  $\Psi^\infty$  near 1 is consistent with the EC regime.  
13  
14  
15  
16  
17  
18  
19  
20  
21  
22

### 23 *2.3.2 Plateau current and foot-of-the-wave analysis for multi-step catalysis at the RDE*

24  
25 Two mechanisms for extracting figures of merit from ECEC' RDE voltammograms can be  
26 easily envisioned which build off the plateau current analysis discussed in section 1.2 as well as the  
27 powerful foot-of-the wave analysis which was recently developed for the analysis of stationary cyclic  
28 voltammograms. The convergence of the Nernst Diffusion Layer approach and the Hale approach  
29 under pure kinetic conditions in the absence of substrate consumption (see Section 1.3.1 and SI-3,  
30 Supporting Information I) allows us to use the Nernst Diffusion Layer approach to derive explicit  
31 equations describing the plateau current and the current at the foot of the wave for an ECEC'  
32 mechanism at the RDE (SI-4, Supporting Information I).  
33  
34  
35  
36  
37  
38  
39  
40  
41

42 Frameworks for interpreting kinetic information from the plateau current as well as the half-  
43 wave potential of steady-state catalytic responses have been rigorously derived for a variety of two-  
44 electron, two-step reaction schemes in the context of stationary voltammetry.<sup>52</sup> For multi-step  
45 reactions, the observed rate constant is still directly determined from the plateau current per equation  
46 2, however the exact rate constant reflected by  $k_{\text{obs}}$  will vary by mechanism. Our derivations in SI-4,  
47 Supporting Information I show that plateau current analysis for the ECEC' reaction can be directly  
48 transposed from stationary CV to RDEV such that equation 2 describes the limiting plateau current  
49  
50  
51  
52  
53  
54  
55  
56  
57  
58  
59  
60

1 of an RDE voltammogram. However, differences in experimental set-ups render plateau current  
2 analysis impractical for the analysis of  $\text{Co}(\text{dmgBF}_2)_2(\text{CH}_3\text{CN})_2$  when working with *para*-substituted  
3 aniliniums in acetonitrile. As mentioned above, this tool can only be applied when a rotation rate-  
4 independent current, representing the kinetic current in the absence of mass transfer effects, is  
5 reached.<sup>36,52</sup> Reaching this regime requires balancing the need for fast kinetics and a sufficiently large  
6 excess of substrate such that substrate consumption can be considered negligible.<sup>14</sup> The need for a  
7 sufficiently large excess factor can pose a serious challenge when using the high solution volumes  
8 (in this case 100 mL) required for many RDE set-ups to ensure that the electrode is both adequately  
9 submerged in the solution and sufficiently distant from the cell bottom to avoid turbulence. This  
10 obstacle is further compounded by the propensity of the solution to evolve over the course of multiple  
11 trials (see section 3.1) which imposes the additional requirement that a new solution be used for each  
12 measurement to ensure accurate results. While this may not be problematic when evaluating HER  
13 under aqueous conditions, it presents severe limitations when working in organic solvents with  
14 anilinium acids. For one, it would require extensive preparation of substrate to be able to conduct the  
15 trials necessary to confirm the plateau current is rotation rate-independent and ensure reproducibility  
16 of the results. In light of the recent global acetonitrile shortage, these large solvent requirements also  
17 bring the question of sustainability to the fore.

18  
19  
20  
21  
22  
23  
24  
25  
26  
27  
28  
29  
30  
31  
32  
33  
34  
35  
36  
37  
38  
39  
40  
41  
42  
43  
44  
45  
46  
47  
48  
49  
50  
51  
52  
53  
54  
55  
56  
57  
58  
59  
60

Thankfully, the excellent progress made over the past decade towards modelling and extracting figures of merit from stationary voltammograms now allow kinetic information to be derived even when competing side phenomena make access to the idealized kinetic current impractical or impossible. Foot-of-the-wave analysis (FOWA), developed by Savéant and Costentin, provides a means of extracting kinetic and mechanistic information from non-ideal stationary voltammograms by using the foot of the wave, where the impact of side phenomena are minimized, to extrapolate the plateau current of the idealized, steady-state catalytic response.<sup>52,73</sup> While this procedure was originally developed for stationary CV, it can be readily extended to RDEV for the ECEC' mechanism.

1 The FOWA procedure for stationary CV, along with enumeration of the conditions under which  
 2 it can be applied, have been reviewed elsewhere.<sup>10,16,53</sup> Briefly, the idealized, steady-state catalytic  
 3 response has been mathematically described for a variety of two-electron, two-step catalytic  
 4 mechanisms.<sup>52</sup> Dividing these idealized equations by the Randles-Sevcik equation, which describes  
 5 the peak current of a homogeneous, diffusion controlled redox reaction ( $i_{\text{peak}}$ ), generates a function  
 6 which linearly depends on  $1/(1 + \exp[\theta])$ . The experimentally obtained catalytic response ( $i_c$ ) is  
 7 divided by  $i_{\text{peak}}$  and this  $i_c/i_{\text{peak}}$  ratio is plotted as a function of  $1/(1 + \exp[\theta])$ . For the ECEC' mechanism  
 8 (with  $E_1 < E_2$ ), these FOWA plots will be linear near the foot of the wave and the slope of this region  
 9 can be used to extract  $k_{\text{FOWA}}$ , which will reflect the rate constant for the first chemical step ( $k_1$ ).

10 A modified procedure was developed to transpose FOWA to RDEV (SI-4, Supporting  
 11 Information I). The Randles-Sevcik equation was replaced with the Levich equation, which describes  
 12 the plateau current ( $i_p$ ) at a RDE for a homogeneous redox reaction. This normalization trick allows  
 13 FOWA to be performed without measuring the electrode surface area. It is not necessary to derive  
 14 new relationships to mathematically describe the idealized catalytic response because these  
 15 equations reflect the steady-state catalytic response. For an ECEC' mechanism where the second  
 16 electron transfer is more thermodynamically favorable than the first and the first chemical step is not  
 17 rate-limiting, the current-potential response can be estimated by equation 5 at  $E \gg E^{o'}$ .<sup>52</sup> Dividing  
 18 equation 5 by the plateau current for the one-electron reduction of  $\text{Co}(\text{dmg}_2\text{BF}_2)_2(\text{CH}_3\text{CN})_2$  ( $i_p$ ), as  
 19 described by the Levich equation (equation 6), yields equation 7.

$$i_c = 2FAC_p^0 \sqrt{k_{\text{FOWA}} D_{\text{cat}}} \left[ \frac{1}{1 + \exp[\theta]} \right] \quad (5)$$

$$i_p = 0.620nFAD^{2/3} \nu^{-1/6} \omega^{1/2} C_p^0 \quad (6)$$

$$\frac{i_c}{i_p} = \frac{3.22}{n} \nu^{1/6} D^{-1/6} \sqrt{\frac{k_{\text{FOWA}}}{\omega}} \quad (7)$$

20 In line with the normalization procedure discussed above, the experimentally obtained catalytic  
 21 response ( $i_c$ ) would now be divided by the plateau current ( $i_p$ ) instead of the peak current ( $i_{\text{peak}}$ ).  
 22  
 23  
 24  
 25  
 26  
 27  
 28  
 29  
 30  
 31  
 32  
 33  
 34  
 35  
 36  
 37  
 38  
 39  
 40  
 41  
 42  
 43  
 44  
 45  
 46  
 47  
 48  
 49  
 50  
 51  
 52  
 53  
 54  
 55  
 56  
 57  
 58  
 59  
 60

1 Plotting this  $i_c/i_p$  ratio as a function of  $1/(1 + \exp[\theta])$  gives a linear relationship at the foot of the wave  
2  
3  
4 with a slope that reflects  $k_{\text{FOWA}}$ .

5  
6 To the best of our knowledge, this modified form of FOWA has not been previously applied in  
7  
8 RDEV. As such, a series of digital simulations were carried out to evaluate whether FOWA can be  
9  
10 reliably extended to RDE voltammograms for an ECEC' catalytic mechanism (SI-3, Supporting  
11  
12 Information II). These simulations confirm that FOWA can be used to evaluate the rate constant for  
13  
14 the first chemical step, however the accuracy of this  $k_1$  value will heavily depend on two factors: the  
15  
16 difference between the redox potential for the two electron transfers ( $\Delta E = E_2 - E_1$ ) and the ratio of  
17  
18 the two rate constants ( $k_1/k_2$ ). These observations are consistent with the known limitations of FOWA  
19  
20 and are not exclusive to the application of this tool in RDEV.<sup>16</sup>

21  
22  
23 To experimentally evaluate the efficacy of FOWA for RDEV, modified FOWA methodology  
24  
25 was used to estimate  $k_1$  for proton-reduction by  $\text{Co}(\text{dmgBF}_2)_2(\text{CH}_3\text{CN})_2$  in the presence of 4-  
26  
27 trifluoromethoxyanilinium. For RDE voltammograms of  $\text{Co}(\text{dmgBF}_2)_2(\text{CH}_3\text{CN})_2$  with 4-  
28  
29 trifluoromethoxyanilinium, converting the potential axis to  $1/(1 + \exp[\theta])$  and dividing the current by  
30  
31  $i_p$  produced traces that are linear at the foot of the catalytic wave (**Figure 12**). Using equation 6, an  
32  
33 observed rate constant ( $k_{\text{FOWA}}$ ) was extracted from the slope of this linear region which, for an ECEC'  
34  
35 mechanism, will reflect the faster rate constant of the first chemical step. Values for  $k_{\text{FOWA}}$  were found  
36  
37 to linearly correlate with acid concentration, allowing a second order rate constant of  $k_1 = 8.42 \times 10^6$   
38  
39  $\text{M}^{-1} \text{s}^{-1}$  ( $k_{\text{FOWA}} = k_1 C_A^0$ ) to be calculated (SI-3, Supporting Information II). This value is in excellent  
40  
41 agreement with the value determined by FOWA under stationary conditions ( $k_1 = 9.91 \times 10^6 \text{ M}^{-1} \text{ s}^{-1}$ ),  
42  
43 supporting the extension of FOWA to RDEV for an ECEC' mechanism.<sup>42</sup>

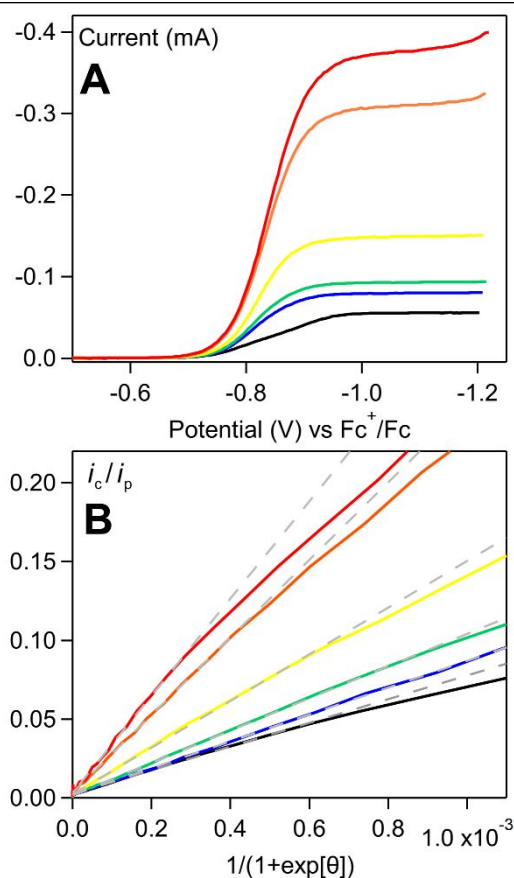


**Figure 12 (A)** RDE voltammograms of 0.5 mM  $Co(dmgbF_2)_2(CH_3CN)_2$  in the absence of acid (grey) and in the presence of 0.181 (black), 0.5 (blue), 0.55 (green), 1 (yellow), 4 (orange), and 5.5 (red) mM 4-trifluoromethoxyanilinium. All voltammograms obtained in 0.25 M  $[NBu_4][PF_6]$  acetonitrile at  $0.01 \text{ V s}^{-1}$  and recorded at  $42 \text{ rad sec}^{-1}$ . **(B)** FOW plot obtained by converting the current to the  $i_c/i_p$  ratio and converting potential to the FOW axis  $1/(1+\exp[\theta])$ . Solid lines represent converted trace and are color-coded to correspond with their RDE voltammogram. Grey dashed are the linear fit of the foot of the wave. FOWA plot expanded to focus on linear region at the foot of the wave.

### 2.3.3 Avenues for future work

$E_{1/2}-\lambda$  relationships have been shown to afford important mechanistic and kinetic information for a number of homogeneous chemical reactions at the RDE, however these derivations have been limited to unimolecular first order reactions, bimolecular dimerization reactions, and the EC' catalytic mechanism. While this prevents direct application of these relationships for HER catalysts, these tools could be analytically or empirically extended to the more complex reaction pathways operative in fuel-

1 forming reactions. This work identified two specific sub-sets of peak shift analysis relevant for the  
2 analysis of ECEC' mechanisms.  
3  
4

5 The first is peak shift analysis of total catalysis waveforms. While it is not anticipated that the  
6 relations derived for the EC' catalytic mechanism (equations 3,4) can be directly transposed to multi-  
7 step processes, comparable equations relating  $E_{1/2}$  to  $\lambda$  are anticipated, akin to what has been derived  
8 for the stationary analogue of peak shift analysis.<sup>42,59</sup> Digital simulations show the existence of a total  
9 catalysis regime in which a catalytic wave with an  $E_{1/2}$  value that varies as a function of  $\lambda$  can be  
10 resolved at potentials positive of the catalyst's redox couple (**Figure 4** and SI-3, Supporting  
11 Information I). It is beyond the scope of this work to develop a generalized and quantitative framework  
12 for peak shift analysis in the total catalysis regime for ECEC' reactions, however it remains an area  
13 of active interest. It is worth noting that preliminary *in silico* work on this topic has shown that the total  
14 catalysis waveform is incredibly sensitive to the ratios of the rate constants for the chemical steps,  
15 the potential separation between electron transfer steps, as well as the standard heterogeneous rate  
16 constant (**Figure 5** and SI-3, Supporting Information I).  
17  
18  
19  
20  
21  
22  
23  
24  
25  
26  
27  
28  
29  
30

31 The second subset of peak shift analysis relates to multi-step catalytic reactions where  $k_1$  is  
32 so slow that the second electron transfer doesn't occur (EC limiting regime). As discussed above,  
33 variable rotation rate trials with 1 equivalent 4-methoxyanilinium displayed behavior consistent with  
34 the EC limiting regime. The half-wave potential of these voltammograms were found to vary linearly  
35 as a function of rotation rate for  $\omega > 42 \text{ rad sec}^{-1}$  (**Figure 13**). A quantitative framework for extracting  
36 kinetic information from the variation in half-wave potential have been derived for second order, non-  
37 catalytic EC reactions; however the chemical step modelled in these derivations was a bimolecular  
38 dimerization and thus these relationships are not directly applicable to bimolecular chemical reactions  
39 between a catalyst and a substrate.<sup>24,35,49</sup> While this makes analytical derivation of an  $E_{1/2}-\lambda_1$   
40 relationships untenable without extreme approximation, the empirical extension of these equations  
41 would be an interesting avenue of future study.  
42  
43  
44  
45  
46  
47  
48  
49  
50  
51  
52  
53  
54  
55  
56  
57  
58  
59  
60

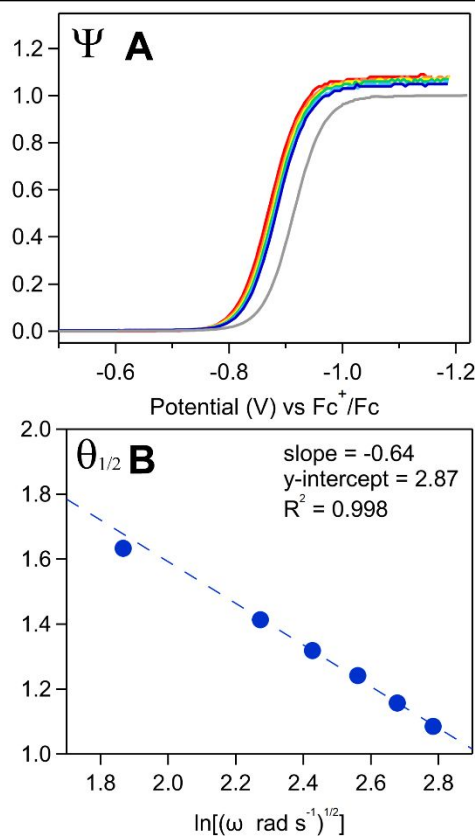


**Figure 13 (A)** RDE voltammograms of 0.5 mM  $\text{Co}(\text{dmgbF}_2)_2(\text{CH}_3\text{CN})_2$  in the absence of acid (grey) and in the presence of 0.5 mM 4-methoxyanilinium at rotation rates of 42 (red), 94 (orange), 128 (yellow), 168 (green), 212 (light blue), and 262  $\text{rad sec}^{-1}$  (blue) with the vertical axis converted to dimensionless current. Voltammograms obtained in 0.25 M  $[\text{NBu}_4][\text{PF}_6]$  acetonitrile at 0.01  $\text{V s}^{-1}$ . **(B)** Plots of  $\theta_{1/2}$  vs  $\ln[\omega^{1/2}]$  for voltammograms of 0.5 mM  $\text{Co}(\text{dmgbF}_2)_2(\text{CH}_3\text{CN})_2$  in the presence of 0.5 mM 4-methoxyanilinium are linear in the rotation rate range 94-262  $\text{rad sec}^{-1}$  where  $\Psi^\infty$  values ranged from 1.06 to 1.04. Experimental data points are denoted by blue circles and the linear fit of the five fastest rotation rates (94-262  $\text{rad sec}^{-1}$ ) shown as a blue dashed line.

### 3. Obstacles to the application of RDEV to homogeneous catalysis

A number of technical challenges beyond those associated with large sample volumes were encountered during formal kinetic analysis of  $\text{Co}(\text{dmgbF}_2)_2(\text{CH}_3\text{CN})_2$  via RDEV. In certain cases, these challenges stemmed from limitations in the equipment design. In others, these challenges were specific to analysis of HER in organic solvents with acid as the proton source. In all cases, these studies highlight the challenges that must be overcome before RDE can become a practical tool for

1 the study of multi-step, homogeneous molecular catalysis as a whole and HER under non-aqueous  
2 conditions in particular. We hope that this rigorous discussion will guide groups working to improve  
3 these electrochemical set-ups and help researchers avoid misinterpretation of RDE data in their own  
4 work.  
5  
6  
7  
8  
9

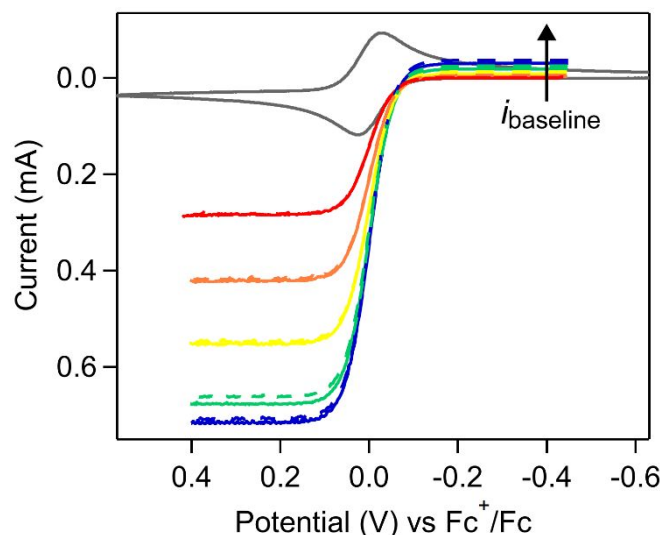
### 10 **3.1 Evolution of solution**

11 One of the major benefits of stationary CV is that it is a non-destructive technique; only the  
12 minute volume of reactants in the reaction layer immediately next to the electrode surface will be  
13 involved in the measurement. From an experimental standpoint, this has the benefit of allowing, in  
14 the absence of catalyst degradation, multiple measurements to be collected in the same solution. For  
15 example, during analysis of  $\text{Co}(\text{dmgBF}_2)_2(\text{CH}_3\text{CN})_2$  with stationary electrochemical techniques,  
16 catalyst decomposition was only observed when working with the stronger *para*-substituted aniliniums  
17 [ $\text{p}K_{\text{a}}(\text{CH}_3\text{CN}) = 7.0\text{-}8.62$ ] and a fresh solution was only required for each voltammetric scan when  
18 working under these conditions.<sup>42</sup> However, we were concerned that the redox intermediates  
19 generated at the electrode surface and subsequently swept into the bulk solution could accumulate  
20 to such appreciable levels that observable changes in the composition of the solution would take  
21 place over the course of multiple RDE voltammograms.  
22  
23  
24  
25  
26  
27  
28  
29  
30  
31  
32  
33  
34

35 To determine whether detectable quantities of redox active species can accumulate in the  
36 bulk solution under experimentally relevant conditions, RDE voltammograms were collected in a Fc-  
37 only solution at five rotation rates and open circuit potential (OCP) measurements were obtained  
38 between each voltammogram. During these voltammograms, the potential was first scanned  
39 positively until a limiting cathodic current (corresponding to the oxidation of ferrocene) was reached  
40 (ca. 0.4 V) at which point the scan direction was switched and the potential was scanned negatively  
41 until a baseline current was reached (ca. -0.45 V). OCP is a powerful metric for tracking solution  
42 composition as it can be directly related to the ratio of  $\text{Fc}^+$  and Fc using the Nernst equation.<sup>13</sup> Over  
43 the course of these trials, the OCP monotonically increased from -0.144 to -0.074 V vs  $\text{Fc}^{+/0}$ ,  
44 corresponding to a 5.4% increase in the concentration of  $\text{Fc}^+$ . This change is concurrent with a  
45  
46  
47  
48  
49  
50  
51  
52  
53  
54  
55  
56  
57  
58  
59  
60



1 cathodic increase in  $i_{\text{baseline}}$  as well as an observable color change of the solution from orange to light  
2 green (Figure 14 and SI-4, Supporting Information II).  
3  
4



5  
6  
7  
8  
9  
10  
11  
12  
13  
14  
15  
16  
17  
18  
19  
20  
21  
22  
23  
24 **Figure 14** RDE voltammograms of 2 mM ferrocene were collected at 5 rotation rates: 42 (red), 94 (orange),  
25 168 (yellow), 262 (green), and 316 (blue) rad sec<sup>-1</sup>. Three voltammograms were recorded at each rotation rate  
26 – first (solid line) and third (dashed line) voltammograms are shown, second voltammogram omitted for clarity.  
27 RDE voltammograms recorded at 0.005 V s<sup>-1</sup> in 0.25 mM [NBu<sub>4</sub>][PF<sub>6</sub>] acetonitrile and OCP measurements were  
28 collected between voltammograms. Stationary voltammogram (grey trace) collected at 0.05 V s<sup>-1</sup> prior to RDE  
29 trials.  
30  
31  
32  
33  
34  
35

36  
37 Quantitative analysis of these voltammograms and OCP measurements indicates that the  
38 cathodic increase in baseline current is a direct result of accumulating [Fc<sup>+</sup>] in the bulk solution. For  
39 one,  $i_{\text{baseline}}$  (after normalizing for  $\omega^{1/2}$ ) directly correlates with the [Fc<sup>+</sup>]/[Fc] ratio determined from the  
40 OCP measurement taken *directly prior* to the voltammogram (Figure 15A). Moreover, the [Fc<sup>+</sup>]/[Fc]  
41 ratio linearly depends on the total charge passed prior to the OCP measurement (Figure 15B).  
42 Satisfyingly, plotting the total moles of oxidized ferrocene as a function of total charge passed gives  
43 a linear dependence with a slope close to the ideal proportionality: moles electrolyzed =  $\frac{Q}{nF}$  (Figure  
44 15C).<sup>12</sup>  
45  
46  
47  
48  
49  
50  
51  
52  
53  
54  
55  
56  
57  
58  
59  
60

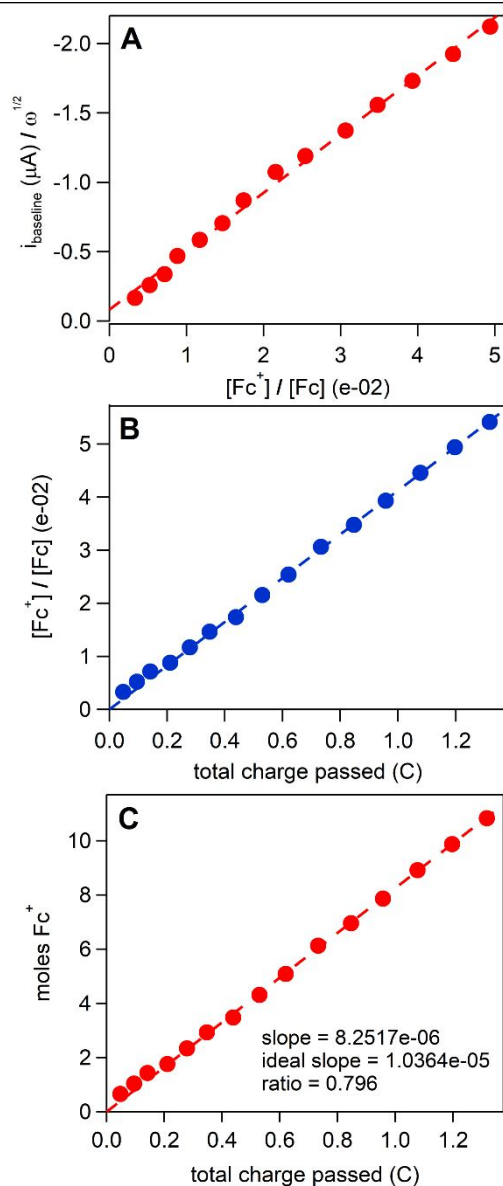


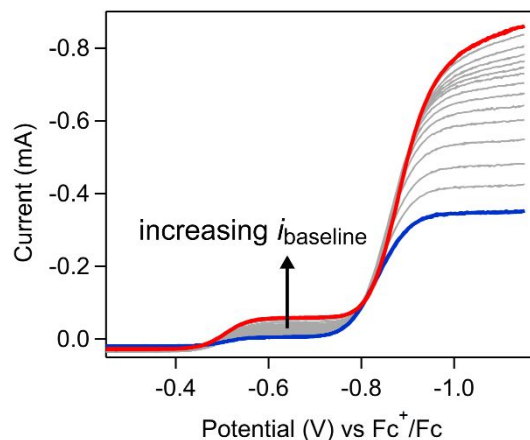
**Figure 15** Data extracted from RDE voltammograms and OCP measurements obtained in 2 mM Fc in 0.25 M  $[\text{NBu}_4][\text{PF}_6]$  acetonitrile. Three voltammograms were collected at each rotation rate where the potential was swept from  $-0.45$  V to  $0.4$  V back to  $-0.45$  V. OCP was related to the ratio of  $[\text{Fc}^+]/[\text{Fc}]$  using the Nernst equation:

$$E = E_{1/2} + \frac{RT}{nF} \ln \left( \frac{[\text{Fc}^+]}{[\text{Fc}]} \right).$$

(A) Rotation rate-normalized baseline current for RDE voltammograms plotted as a function of the  $[\text{Fc}^+]/[\text{Fc}]$  ratio determined from the OCP measurement taken directly prior to the start of the voltammogram. (B) The ratio of  $[\text{Fc}^+]/[\text{Fc}]$  determined via OCP as a function of the charge passed in all previous RDE voltammograms. (C) The moles of  $\text{Fc}^+$  linearly depends on the total charge passed during all prior scans with a slope of  $8.25\text{e-}06$  mol  $\text{C}^{-1}$ , which is in reasonably good agreement with the predicted value of  $(1/nF)$ .

1  
2 Similar deviations in the baseline current were observed under catalytic conditions. For RDE  
3  
4 voltammograms collected in a fresh solution of  $\text{Co}(\text{dmgBF}_2)_2(\text{CH}_3\text{CN})_2$  and acid with a Fc or Fc\*  
5  
6 internal standard, little to no current is passed between the catalytic wave and the  $\text{Fc}^{+/0}$  or  $\text{FcCp}^*_{2+/0}$   
7  
8 couple, as expected for a system where the Co(II) form of  $\text{Co}(\text{dmgBF}_2)_2(\text{CH}_3\text{CN})_2$  and the neutral form  
9  
10 of Fc or Fc\* are the only redox active analytes. For subsequent voltammograms collected in the same  
11  
12 solution, additional cathodic current was consistently observed in this potential range, consistent with  
13  
14 the accumulation of  $\text{Fc}^+$  or  $\text{Fc}^{*+}$  (**Figure 16**). Accumulation of oxidized internal standard was also  
15  
16 observed spectroscopically under catalytic conditions (SI-4, Supporting Information II).  
17

18  
19 Taken together, these experiments show that redox active species generated at the RDE  
20  
21 surface and subsequently swept into solution can alter the composition of the solution to such a  
22  
23 degree that it influences the current-potential response, in these instances manifesting as an increase  
24  
25 in  $i_{\text{baseline}}$ . These results further emphasize the need for RDE set-ups which require small sample  
26  
27 volumes (and thus can be replaced between scans) if RDEV is to be practical for the study of  
28  
29 homogeneous molecular catalysis.  
30



46 **Figure 16** RDE voltammograms of 0.5 mM  $\text{Co}(\text{dmgBF}_2)_2(\text{CH}_3\text{CN})_2$  with 5 mM 4-trifluoromethoxyanilinium and  
47  
48 0.5 mM decamethylferrocene. Rotation rates increased from 42 (blue) to 513 (red)  $\text{rad sec}^{-1}$ . Cyclic  
49  
50 voltammograms started at -0.25 V and recorded at  $0.01 \text{ V sec}^{-1}$  in 0.25 M  $[\text{NBu}_4][\text{PF}_6]$  acetonitrile.  
51

### 3.2 Modification of electrode surface

An important consideration during any electrochemical study is the possibility of deleterious deposition reactions that result in modification of the electrode surface. In the homogeneous electrocatalysis literature, the most commonly reported class of electrodeposition reactions involve the transformation of a molecular precatalyst into a heterogeneous, electrode-adsorbed catalytic material that is no longer molecular in nature.<sup>74</sup> Previous work evaluating the stability of  $\text{Co}(\text{dmgBF}_2)_2(\text{CH}_3\text{CN})_2$  has shown that while deposition of a weakly-adsorbed cobalt material is possible under reducing and protic conditions, this reactivity only occurs when employing strong acids (ex.  $[\text{DMFH}][\text{OTF}]$ ,  $\text{p}K_a = 6.1$  in  $\text{CH}_3\text{CN}$ ).<sup>75</sup> Less well discussed is the case where deposition of a non-catalytic material during catalytic trials leads to changes in the electrode surface area, morphology, or electron transfer kinetics.<sup>76</sup> One particularly pertinent example of this reactivity involves the electrochemical reduction of certain Brønsted acids by glassy carbon electrodes which has been reported to generate an insulating film which can drastically inhibit electron transfer kinetics.<sup>41,77</sup>

To assess the potential impact of acid-induced electrode fouling on catalytic voltammograms, a series of RDE voltammograms were collected in an electrolyte solution containing only 4-trifluoromethoxyanilinium (and ferrocene as an internal standard). This electrode was then rinsed and used to collect a catalytic voltammogram under stationary conditions in a solution of 0.5 mM  $\text{Co}(\text{dmgBF}_2)_2(\text{CH}_3\text{CN})_2$  with 5 mM 4-trifluoromethoxyanilinium. Comparing these results to catalytic voltammograms collected with a freshly pretreated electrode shows a drastic increase in the peak-to-peak separation of the  $\text{Co}^{\text{III/II}}$  couple ( $\Delta E_p[\text{Co}^{\text{III/II}}]$ ) (an additional redox couple of  $\text{Co}(\text{dmgBF}_2)_2(\text{CH}_3\text{CN})_2$  which is not relevant to catalysis), behavior consistent with a decrease in the  $k_s$  value for this couple (**Figure 17**). These results indicate that interactions between the acid and the electrode surface under reducing conditions can lead to a passivating surface deposit.<sup>12,24</sup>

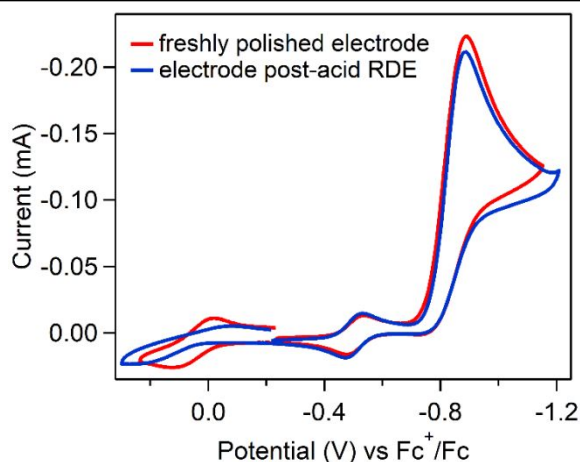


**Figure 17** Stationary cyclic voltammogram of 0.5 mM  $\text{Co}(\text{dmgbF}_2)_2(\text{CH}_3\text{CN})_2$  in the presence of 5 mM 4-trifluoromethoxyanilinium collected with a freshly polished working electrode (red) contains a reversible  $\text{Co}^{\text{III/II}}$  couple ( $E_{1/2} = 0.075$  V). This feature is replaced by an irreversible wave for catalytic voltammograms recorded with working electrodes previously subjected to variable rotation rate studies in a solution of 4-trifluoromethoxyanilinium (blue). Voltammograms recorded at  $0.1 \text{ V s}^{-1}$  in 0.25 M  $[\text{NBu}_4][\text{PF}_6]$  acetonitrile using a decamethylferrocene internal standard [ $E^0(\text{Fc}^{*+/0}) = -0.505$  V].

To probe whether this deposition was relevant under catalytic conditions, variable rotation rate trials were conducted in a solution of 0.5 mM  $\text{Co}(\text{dmgbF}_2)_2(\text{CH}_3\text{CN})_2$  with 5 mM 4-trifluoromethoxyanilinium and stationary voltammograms were collected between the RDE voltammograms. These stationary voltammograms show a clear, monotonic increase in  $\Delta E_p[\text{Co}^{\text{III/II}}]$  over the course of the RDE trials (**Figure 18** and SI-5, Supporting Information II), identical to the behavior observed in stationary voltammograms recorded after RDE measurements in an acid only solution (**Figure 17**). This suggests that the properties of the electrode interface can be altered over the course of a *single RDE trial*, a phenomenon not observed during control studies where multiple cycling experiments were conducted under stationary conditions (SI-5, Supporting Information II). A second series of control studies analogous to the RDE trials described for **Figure 17** also suggest that the degree of acid-induced electrode fouling observed after repetitive cycling in the presence of acid is more pronounced in hydrodynamic experiments relative to their stationary counterparts (SI-5, Supporting Information II). While these studies do not elucidate a precise explanation for this difference in behavior between hydrodynamic and stationary conditions, they do serve as a cautionary

tale that great care should be taken when trying to translate experimental guidelines designed for stationary trials to hydrodynamic conditions.

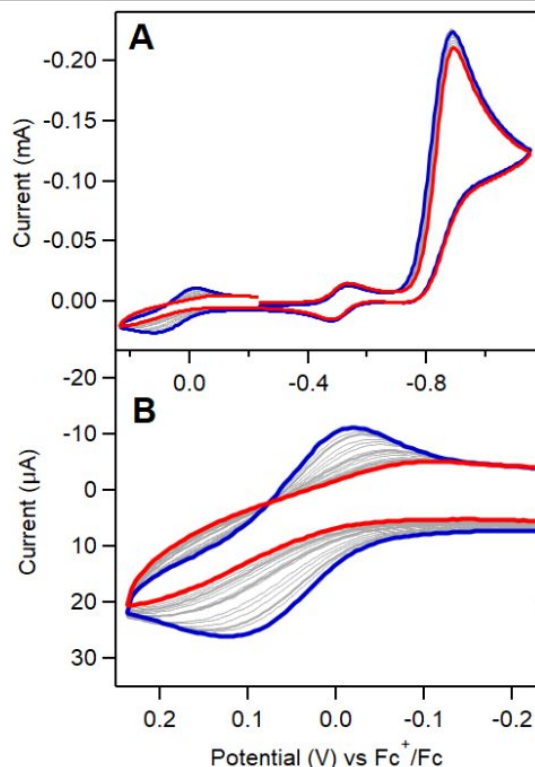


**Figure 18 (A)** Stationary cyclic voltammograms of 0.5 mM  $\text{Co}(\text{dmgbF}_2)_2(\text{CH}_3\text{CN})_2$  with 5 mM 4-trifluoromethoxyanilinium collected before variable rotation rate trials (blue) and after RDE voltammograms obtained at 42 – 513  $\text{rad sec}^{-1}$  (grey to red). Voltammograms obtained at 0.1  $\text{V s}^{-1}$  in 0.25 M  $[\text{NBu}_4][\text{PF}_6]$  acetonitrile using a decamethylferrocene internal standard. **(B)** Expansion of  $\text{Co}^{\text{III/II}}$  redox couple shows monotonic increase in peak separation over the course of the variable rotation rate trials.

Further monitoring electrode properties with stationary voltammetry during variable rotation rate trials with 0.5 mM  $\text{Co}(\text{dmgbF}_2)_2(\text{CH}_3\text{CN})_2$  and 5 mM anilinium yielded results which suggest that more complex reactivity than simple electrode passivation by an acid-related process is taking place (**Figure 19**). In these trials, no increase in  $\Delta E_p[\text{Co}^{\text{III/II}}]$  is initially observed. Instead, the peak current for the catalytic feature initially increases in magnitude, behavior similarly observed in voltammograms collected with 5 mM 4-methoxyanilinium (SI-5, Supporting Information II). After some number of scans, the peak current in the stationary voltammograms begins to decrease, a phenomenon accompanied by an increase in  $\Delta E_p[\text{Co}^{\text{III/II}}]$ . A preliminary postulate is that deposition initially manifests

as an apparent increase in electroactive surface area which, upon reaching some critical mass or geometric specifications, results in an apparent decrease in the heterogeneous electron transfer rate constant, however more rigorous evaluation of this phenomena is required before definitive conclusions can be drawn.

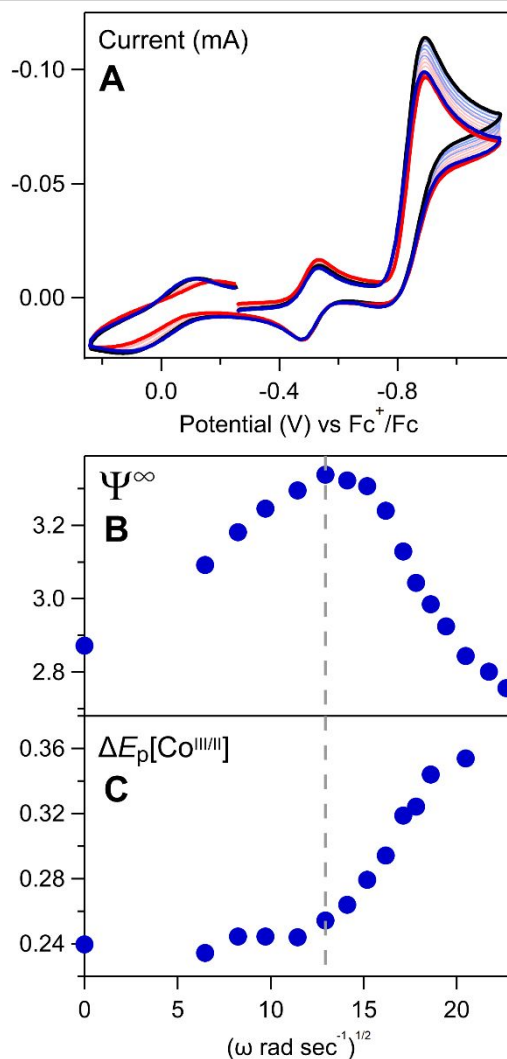


**Figure 19 (A)** Stationary voltammograms of 0.5 mM  $\text{Co}(\text{dmgBF}_2)_2(\text{CH}_3\text{CN})_2$  in the presence of 5 mM anilinium collected before RDE trials (dark blue trace), after RDE trials (dark red), and in between each RDE trial during variable rotation rate studies. Stationary voltammograms divided into 3 subsets: voltammograms collected after trials at  $\omega = 42\text{--}131$  (light blue), 168 (black), and 199–513  $\text{rad sec}^{-1}$  (light red). Voltammograms obtained at 0.1  $\text{V s}^{-1}$  in 0.25 M  $[\text{NBu}_4][\text{PF}_6]$  acetonitrile using a decamethylferrocene internal standard. **(B)**  $\Psi^\infty = i_c/i_{peak}$  values for the catalytic wave and **(C)** and  $\Delta E_p$  values for the  $\text{Co}^{\text{III/II}}$  couple as a function of the rotation rate for the RDE

1 trial collected prior to the stationary voltammogram. Rotation rates were traversed in ascending order, such that  
2 moving from left to right across the x-axis represents both an increase in  $\omega$  and trial number. Grey dashed line  
3 represents the voltammogram collected after the RDE trial at 168 rad sec<sup>-1</sup>, corresponding to the black trace in  
4 panel A, and demarcates the onset of observable electrode passivation. For voltammograms collected prior to  
5 this trial, an increase in  $\psi^\infty$  is observed with little to no change in  $(\Delta E_p[\text{Co}^{\text{III/II}}])$ . For all voltammograms collected  
6 subsequent to this trial, a decrease in  $\psi^\infty$  and a monotonic increase in  $\Delta E_p[\text{Co}^{\text{III/II}}]$  is observed.

---

### 14 3.3 Inclined plateau currents introduce quantitative uncertainty

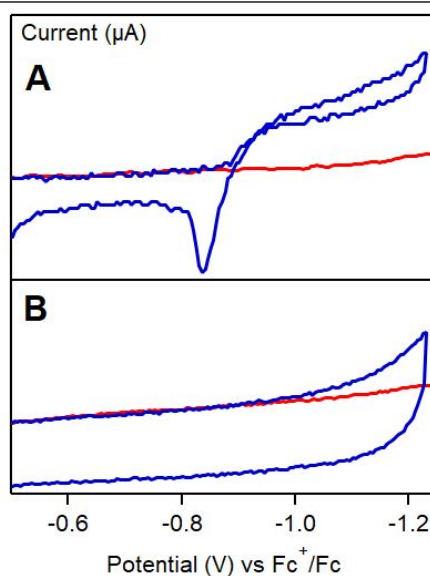
16 A challenge commonly encountered during this work was the failure to achieve a flat plateau  
17 current during catalytic trials, with current-potential responses instead exhibiting an inclined plateau  
18 that never reached a potential-independent current value (**Figure 16**). The inability to reach limiting  
19 plateau currents is not uncommon in RDEV, with imperfections in the equipment (e.g. cell, rotator,  
20 electrode) commonly invoked as the source of this problem. For all rotation rates used in this work, it  
21 was possible to achieve limiting plateau currents when evaluating simple electron transfer with  
22  $\text{Co}(\text{dmgBF}_2)_2(\text{CH}_3\text{CN})_2$  in the absence of acid (**Figure 8**), making it highly unlikely that the inclined  
23 plateaus stemmed from equipment defects.

33 While we were not able to diagnose the exact reactivity underpinning this phenomenon, a few  
34 possibilities were identified. One possibility is that electrodeposition increases the effective electrode  
35 surface area during the potential sweep, behavior consistent with the initial apparent increase in  
36 electrode area observed in stationary voltammograms collected between RDE voltammograms  
37 during variable rotation rate trials for  $\text{Co}(\text{dmgBF}_2)_2(\text{CH}_3\text{CN})_2$  with anilinium and 4-methoxyanilinium  
38 (**Figure 19** and SI-5, Supporting Information II). An alternative explanation is that these sloping  
39 plateaus stem from contributions to the catalytic current from direct reduction of acid at the electrode  
40 surface.<sup>78</sup> The latter explanation is in line with earlier models which propose that inclined plateau  
41 currents are a direct results of reactivity intrinsic to heterogeneous catalytic systems.<sup>79</sup>

52 All acids used in this work had been previously shown to undergo direct reduction at potentials  
53 substantially negative of the catalytic wave of  $\text{Co}(\text{dmgBF}_2)_2(\text{CH}_3\text{CN})_2$  under stationary conditions.<sup>41</sup>



1  
2 However, analysis of acid electroreduction by RDEV indicates that guidelines developed for  
3 stationary set-ups cannot be directly translated to RDEV. The onset of acid reduction in RDE  
4 voltammograms can be clearly identified at more positive potentials compared to trials under  
5 stationary conditions; behavior observed for both *para*-substituted aniliniums (**Figure 20**) and non-  
6 anilinium acids (SI-6, Supporting Information II).  
7  
8  
9  
10  
11



12  
13  
14  
15  
16  
17  
18  
19  
20  
21  
22  
23  
24  
25  
26  
27  
28  
29  
30 **Figure 20 (A)** RDE voltammogram of 1.25 mM 4-trifluoromethoxyanilinium recorded at 377 (blue) rad sec<sup>-1</sup>  
31 overlaid with the background scan collected in 0.25 M [NBu<sub>4</sub>][PF<sub>6</sub>] acetonitrile (red). Voltammograms obtained  
32 at 0.01 V s<sup>-1</sup> using a ferrocene internal standard. We have not identified the sharp feature observed on the  
33 anodic scan at E<sub>p</sub> ~ 0.85V vs. Fc<sup>+0</sup>, but note it is consistent with deposition of a heterogeneous species on the  
34 electrode surface (see 3.2).<sup>74</sup> **(B)** Stationary cyclic voltammograms of 1.25 mM 4-trifluoromethoxyanilinium  
35 (blue) overlaid with the background scan collected in 0.25 M [NBu<sub>4</sub>][PF<sub>6</sub>] acetonitrile (red). Voltammograms  
36 recorded at 0.1 V s<sup>-1</sup> using a ferrocene internal standard.  
37  
38  
39  
40  
41  
42  
43

44  
45 In RDEV, the extent that direct reduction impacts the electrochemical response will depend  
46 on the relative kinetics of homogeneous catalysis and the electrode process, making it challenging to  
47 tease apart the relative contributions of the two processes. For fast homogeneous catalysis and slow  
48 direct reduction of acid, kinetic analysis will likely be unencumbered by direct reduction current.  
49 However, if direct reactivity at the electrode surface is not negligible, it can skew both the magnitude  
50 and shape of the waveform, resulting in an inclined plateau current that does not reach a potential-  
51  
52  
53  
54  
55  
56  
57  
58  
59  
60

1 independent value. Without appropriate methods for deconvoluting the contribution of the two  
2 processes, it is challenging to objectively extract a plateau current and quantitatively analyze data.  
3  
4 Given the importance of Brønsted acids as a proton source when evaluating molecular hydrogen  
5 evolution electrocatalysts in organic solvents, serious evaluation of direct acid reduction at the RDE  
6 surface is warranted before RDEV can be rigorously used to study molecular HER catalysts in non-  
7 aqueous conditions.  
8  
9

## 14 CONCLUSIONS

16 Characterizing and quantifying the complex reactivity underpinning multi-step electrocatalysis  
17 requires advanced electrochemical techniques which can couple catalytic current flow obtained from  
18 voltammetry with real-time detection of products or reactive intermediates. The viability of techniques  
19 based on rotating disc electrodes for the analysis of multi-step, homogeneous fuel-forming reactions  
20 has been explored. Mathematical models for analyzing and digitally simulating RDE voltammograms  
21 for the ECEC' catalytic mechanism were derived using two strategies based on the Nernst Diffusion  
22 Layer and application of Hale Theory. Digital simulations showed convergence of these models over  
23 a wide range of reaction conditions which allowed plateau current analysis and foot-of-the-wave  
24 analysis – two methodologies commonly used for analysis of stationary voltammograms – to be  
25 extended to RDEV.  
26  
27

37 Application of RDE techniques to a well-characterized cobaloxime HER electrocatalyst validated  
38 this theoretical treatment and allowed the viability of RDE techniques for analysis of multistep catalytic  
39 reactions to be evaluated in a real-world setting and compared to stationary electrochemical methods.  
40 While both stationary and RDE measurements yield similar quantitative data, experimental obstacles  
41 support the use of stationary electrochemical methods for primary analysis of homogeneous HER  
42 electrocatalysis under non-aqueous conditions. These results also highlight the clear need for  
43 accessible and affordable small volume RDE set-ups for this tool to be practical on a large scale.  
44  
45

52 Three additional obstacles to the application of RDEV to homogeneous HER catalyst under non-  
53 aqueous conditions were identified: (1) redox intermediates swept into the bulk solution can alter the  
54 solution composition and impact voltammetric data; (2) interactions between common acids and  
55  
56  
57  
58

1  
2 glassy carbon can passivate the electrode surface during RDE trials; (3) the inability to achieve flat  
3  
4 plateau currents – likely due to contributions from direct substrate reduction – hinders accurate  
5  
6 extraction of kinetic data. This theoretical treatment along with the careful consideration of  
7  
8 experimental challenges will hopefully guide the development of cutting-edge electrochemical  
9  
10 techniques and ensure appropriate application of RDE for the characterization of fuel-forming  
11  
12 electrocatalytic reactions.

### 13 14 **CONFLICTS OF INTEREST**

15  
16 None

### 17 18 **ACKNOWLEDGEMENTS**

19  
20 This research was supported by the U.S. Department of Energy, Office of Science, Office of Basic  
21  
22 Energy Sciences, under Award DE-SC0015303. We gratefully acknowledge Dr. Alex Peroff, Dr. Li  
23  
24 Sun, and Dr. Frank Dalton from Pine Research Instrumentation for providing instrumentation, helpful  
25  
26 discussions, and encouragement for this project. J.L.D. acknowledges support from a Packard  
27  
28 Fellowship for Science and Engineering and the Alfred P. Sloan Foundation. K.J.L. acknowledges a  
29  
30 Dissertation Completion Fellowship and a Lampley Graduate Fellowship from the University of North  
31  
32 Carolina. C.T.G. acknowledges a Summer Undergraduate Research Fellowship from the University  
33  
34 of North Carolina.

### 35 36 **FOOTNOTES**

37  
38  
39  
40  
41  
42  
43  
44  
45  
46  
47  
48  
49  
50  
51  
52  
53  
54  
55  
56  
57  
58  
59  
60 None

1  
2 **REFERENCES**

- 3 1 U.S. Global Change Research Program, 2018, **II**, 1–470.
- 4 2 Y. Xu and V. Ramanathan, *Proc. Natl. Acad. Sci.*, 2017, **114**, 10315–10323.
- 5 3 Intergovernmental Panel on Climate Change, *Global warming of 1.5°C*, 2018.
- 6 4 H. B. Gray, *Nat. Chem.*, 2009, **1**, 7–7.
- 7 5 N. S. Lewis and D. G. Nocera, *Proc. Natl. Acad. Sci.*, 2006, **103**, 15729–15735.
- 8 6 P. Denholm, M. O. Connell, G. Brinkman, J. Jorgenson, P. Denholm, M. O. Connell, G.  
9 Brinkman and J. Jorgenson, *Overgeneration from Solar Energy in California : A Field Guide  
10 to the Duck Chart*, 2015.
- 11 7 R. J. Detz, J. N. H. Reek and B. C. C. van der Zwaan, *Energy Environ. Sci.*, 2018, **11**, 1653–  
12 1669.
- 13 8 A. M. Appel, S. Bare, B. M. Bartlett, T. Bligaard, B. D. Chandler and R. J. Davis, in *U.S.  
14 Department of Energy, Office of Basic Energy Sciences Workshop*, Gaithersburg, Maryland,  
15 2017.
- 16 9 D. L. DuBois, *Inorg. Chem.*, 2014, **53**, 3935–3960.
- 17 10 K. J. Lee, N. Elgrishi, B. Kandemir and J. L. Dempsey, *Nat. Rev. Chem.*, 2017, **1**, 0039.
- 18 11 B. H. Solis and S. Hammes-Schiffer, *Inorg. Chem.*, 2014, **53**, 6427–6443.
- 19 12 A. J. Bard and L. R. Faulkner, *Electrochemical Methods: Fundamentals and Applications*,  
20 John Wiley & Sons, Inc., Hoboken, NJ, USA, 2nd edn., 2001.
- 21 13 N. Elgrishi, K. J. Rountree, B. D. McCarthy, E. S. Rountree, T. T. Eisenhart and J. L.  
22 Dempsey, *J. Chem. Educ.*, 2018, **95**, 197–206.
- 23 14 J.-M. Savéant, *Elements of Molecular and Biomolecular Electrochemistry*, John Wiley &  
24 Sons, Inc., Hoboken, NJ, USA, 2006.
- 25 15 L. I. Stephens and J. Mauzeroll, *J. Chem. Educ.*, 2019, **96**, 2217–2224.
- 26 16 V. C.-C. Wang and B. A. Johnson, *ACS Catal.*, 2019, **9**, 7109–7123.
- 27 17 C. Costentin, H. Dridi and J.-M. Savéant, *J. Am. Chem. Soc.*, 2014, **136**, 13727–13734.
- 28 18 Y. B. Vogel, A. Molina, J. Gonzalez and S. Ciampi, *Anal. Chem.*, 2019, **91**, 5929–5937.
- 29 19 Y. S. Kim, V. Balland, B. Limoges and C. Costentin, *Phys. Chem. Chem. Phys.*, 2017, **19**,  
30 17944–17951.
- 31 20 C. Costentin and D. G. Nocera, *J. Phys. Chem. C*, 2019, **123**, 1966–1973.
- 32 21 E. O. Barnes, G. E. M. Lewis, S. E. C. Dale, F. Marken and R. G. Compton, *Analyst*, 2012,  
33 **137**, 1068.
- 34 22 R. G. Compton, E. Laborda and K. R. Ward, *Understanding Voltammetry: Simulation of  
35 Electrode Processes*, IMPERIAL COLLEGE PRESS, 2014.
- 36 23 V. G. Levich, *Physicochemical Hydrodynamics*, Prentice-Hall, Englewood Cliffs, NJ, USA,  
37 1962.
- 38 24 R. G. Compton and C. E. Banks, *Understanding Voltammetry*, Imperial College Press,

- 1 London, 2nd edn., 2011.
- 2
- 3 25 C. E. Banks, A. O. Simm, R. Bowler, K. Dawes and R. G. Compton, *Anal. Chem.*, 2005, **77**,
- 4 1928–1930.
- 5
- 6 26 A. Frumkin, L. Nekrasov, B. Levich and J. Ivanov, *J. Electroanal. Chem.*, 1959, **1**, 84–90.
- 7
- 8 27 D. G. H. Hetterscheid, *Chem. Commun.*, 2017, **53**, 10622–10631.
- 9
- 10 28 J. J. Concepcion, R. A. Binstead, L. Alibabaei and T. J. Meyer, *Inorg. Chem.*, 2013, **52**,
- 11 10744–10746.
- 12
- 13 29 C. Costentin, H. Dridi and J.-M. Savéant, *J. Am. Chem. Soc.*, 2015, **137**, 13535–13544.
- 14
- 15 30 S. Kishioka and A. Yamada, *J. Electroanal. Chem.*, 2005, **578**, 71–77.
- 16
- 17 31 S. Kishioka and A. Yamada, *Electrochim. Acta*, 2006, **51**, 4582–4588.
- 18
- 19 32 N. D. Schley, J. D. Blakemore, N. K. Subbaiyan, C. D. Incarvito, F. D'Souza, R. H. Crabtree
- 20 and G. W. Brudvig, *J. Am. Chem. Soc.*, 2011, **133**, 10473–10481.
- 21
- 22 33 C. C. L. McCrory, C. Uyeda and J. C. Peters, *J. Am. Chem. Soc.*, 2012, **134**, 3164–3170.
- 23
- 24 34 D. Khusnutdinova, B. L. Wadsworth, M. Flores, A. M. Beiler, E. A. Reyes Cruz, Y. Zenkov
- 25 and G. F. Moore, *ACS Catal.*, 2018, **8**, 9888–9898.
- 26
- 27 35 R. G. Compton and P. R. Unwin, *J. Chem. Soc. Faraday Trans. 1 Phys. Chem. Condens.*
- 28 *Phases*, 1989, **85**, 1821.
- 29
- 30 36 S. Treimer, A. Tang and D. C. Johnson, *Electroanalysis*, 2002, **14**, 165.
- 31
- 32 37 R. G. Compton and R. A. Spackman, *J. Electroanal. Chem. Interfacial Electrochem.*, 1990,
- 33 **285**, 273–279.
- 34
- 35 38 C. P. Andrieux, J. M. Dumas-Bouchiat and J. M. Savéant, *J. Electroanal. Chem. Interfacial*
- 36 *Electrochem.*, 1980, **113**, 1–18.
- 37
- 38 39 R. G. Compton, R. A. Spackman and P. R. Unwin, *J. Electroanal. Chem. Interfacial*
- 39 *Electrochem.*, 1989, **264**, 1–25.
- 40
- 41 40 A. Bakac and J. H. Espenson, *J. Am. Chem. Soc.*, 1984, **106**, 5197–5202.
- 42
- 43 41 B. D. McCarthy, D. J. Martin, E. S. Rountree, A. C. Ullman and J. L. Dempsey, *Inorg. Chem.*,
- 44 2014, **53**, 8350–8361.
- 45
- 46 42 E. S. Rountree, D. J. Martin, B. D. McCarthy and J. L. Dempsey, *ACS Catal.*, 2016, **6**, 3326–
- 47 3335.
- 48
- 49 43 R. Saravanakumar, P. Pirabaharan and L. Rajendran, *Electrochim. Acta*, 2019, **313**, 441–
- 50 456.
- 51
- 52 44 J. E. Nolan and J. A. Plambeck, *J. Electroanal. Chem. Interfacial Electrochem.*, 1990, **294**,
- 53 1–20.
- 54
- 55 45 K. B. Prater and A. J. Bard, *J. Electrochem. Soc.*, 1970, **117**, 1517.
- 56
- 57 46 S. Bruckenstein and S. Prager, *Anal. Chem.*, 1967, **39**, 1161–1163.
- 58
- 59 47 D. Haberland and R. Landsberg, *Berichte der Bunsengesellschaft*, 1966, 724–727.
- 60
- 48 R. G. Compton, M. E. Laing, D. Mason, R. J. Northing and P. R. Unwin, *Proc. R. Soc. A*

- 1 *Math. Phys. Eng. Sci.*, 1988, **418**, 113–154.
- 2
- 3 49 R. G. Compton, D. Mason and P. R. Unwin, *J. Chem. Soc. Faraday Trans. 1 Phys. Chem.*
- 4 *Condens. Phases*, 1988, **84**, 473.
- 5
- 6 50 R. G. Compton and R. G. Harland, *J. Chem. Soc. Faraday Trans. I*, 1989, **85**, 761–771.
- 7
- 8 51 C. P. Andrieux, J. M. Dumas-Bouchiat and J. M. Saveant, *J. Electroanal. Chem. Interfacial*
- 9 *Electrochem.*, 1978, **87**, 39–53.
- 10
- 11 52 C. Costentin and J.-M. Savéant, *ChemElectroChem*, 2014, **1**, 1226–1236.
- 12
- 13 53 E. S. Rountree, B. D. McCarthy, T. T. Eisenhart and J. L. Dempsey, *Inorg. Chem.*, 2014, **53**,
- 14 9983–10002.
- 15
- 16 54 J. M. Savéant and K. B. Su, *J. Electroanal. Chem. Interfacial Electrochem.*, 1984, **171**, 341–
- 17 349.
- 18
- 19 55 D. J. Martin, B. D. McCarthy, E. S. Rountree and J. L. Dempsey, *Dalt. Trans.*, 2016, **45**,
- 20 9970–9976.
- 21
- 22 56 P. Delahay and G. L. Stiehl, *J. Am. Chem. Soc.*, 1952, **74**, 3500–3505.
- 23
- 24 57 B. D. McCarthy, C. L. Donley and J. L. Dempsey, *Chem. Sci.*, 2015, **6**, 2827–2834.
- 25
- 26 58 L. A. Clare, T. D. Pham, L. A. Rafou, A. G. Buenaventura, T. R. Scott, V. Mikhaylova and D.
- 27 K. Smith, *J. Phys. Chem. C*, 2019, **123**, 23390–23402.
- 28
- 29 59 C. Costentin, D. G. Nocera and C. N. Brodsky, *Proc. Natl. Acad. Sci.*, 2017, **114**, 11303–
- 30 11308.
- 31
- 32 60 E. Kätelhön and R. G. Compton, *Analyst*, 2015, **140**, 2592–2598.
- 33
- 34 61 W. J. Albery, *Electrode kinetics*, Clarendon Press, 1975.
- 35
- 36 62 J. L. Dempsey, B. S. Brunshwig, J. R. Winkler and H. B. Gray, *Acc. Chem. Res.*, 2009, **42**,
- 37 1995–2004.
- 38
- 39 63 P. Connolly and J. H. Espenson, *Inorg. Chem.*, 1986, **25**, 2684–2688.
- 40
- 41 64 X. Hu, B. M. Cossairt, B. S. Brunshwig, N. S. Lewis and J. C. Peters, *Chem. Commun.*,
- 42 2005, 4723.
- 43
- 44 65 X. Hu, B. S. Brunshwig and J. C. Peters, *J. Am. Chem. Soc.*, 2007, **129**, 8988–8998.
- 45
- 46 66 M. Razavet, V. Artero and M. Fontecave, *Inorg. Chem.*, 2005, **44**, 4786–4795.
- 47
- 48 67 B. H. Solis and S. Hammes-Schiffer, *Inorg. Chem.*, 2011, **50**, 11252–11262.
- 49
- 50 68 J. L. Dempsey, J. R. Winkler and H. B. Gray, *J. Am. Chem. Soc.*, 2010, **132**, 16774–16776.
- 51
- 52 69 J. L. Dempsey, J. R. Winkler and H. B. Gray, *J. Am. Chem. Soc.*, 2010, **132**, 1060–1065.
- 53
- 54 70 J. T. Muckerman and E. Fujita, *Chem. Commun.*, 2011, **47**, 12456.
- 55
- 56 71 I. Kaljurand, A. Kütt, L. Sooväli, T. Rodima, V. Mäemets, I. Leito and I. A. Koppel, *J. Org.*
- 57 *Chem.*, 2005, **70**, 1019–1028.
- 58
- 59 72 C. Baffert, V. Artero and M. Fontecave, *Inorg. Chem.*, 2007, **46**, 1817–1824.
- 60
- 73 C. Costentin, S. Drouet, M. Robert and J.-M. Savéant, *J. Am. Chem. Soc.*, 2012, **134**,

1  
2 11235–11242.

3  
4 74 K. J. Lee, B. D. McCarthy and J. L. Dempsey, *Chem. Soc. Rev.*, 2019, **48**, 2927–2945.

5  
6 75 D. J. Sconyers and J. D. Blakemore, *Chem. Commun.*, 2017, **53**, 7286–7289.

7  
8 76 R. L. McCreery, *Chem. Rev.*, 2008, **108**, 2646–2687.

9  
10 77 R. P. Wong, J. E. Wong and V. I. Birss, *Can. J. Chem.*, 2004, **82**, 1536–1544.

11  
12 78 G. A. N. Felton, C. A. Mebi, B. J. Petro, A. K. Vannucci, D. H. Evans, R. S. Glass and D. L. Lichtenberger, *J. Organomet. Chem.*, 2009, **694**, 2681–2699.

13  
14 79 R. Jiang and F. C. Anson, *J. Electroanal. Chem. Interfacial Electrochem.*, 1991, **305**, 171–  
15 184.

1  
2  
3  
4  
5  
6  
7  
8  
9  
10  
11  
12  
13  
14  
15  
16  
17  
18  
19  
20  
21  
22  
23  
24  
25  
26  
27  
28  
29  
30  
31  
32  
33  
34  
35  
36  
37  
38  
39  
40  
41  
42  
43  
44  
45  
46  
47  
48  
49  
50  
51  
52  
53  
54  
55  
56  
57  
58  
59  
60

